# Semiconductor Nanowires: Characterization and surface modification

Yngman, Sofie

2019

*Document Version:*
Publisher's PDF, also known as Version of record

# Semiconductor Nanowires

## Characterization and surface modification

SOFIE YNGMAN
SYNCHROTRON RADIATION RESEARCH | FACULTY OF SCIENCE | LUND UNIVERSITY

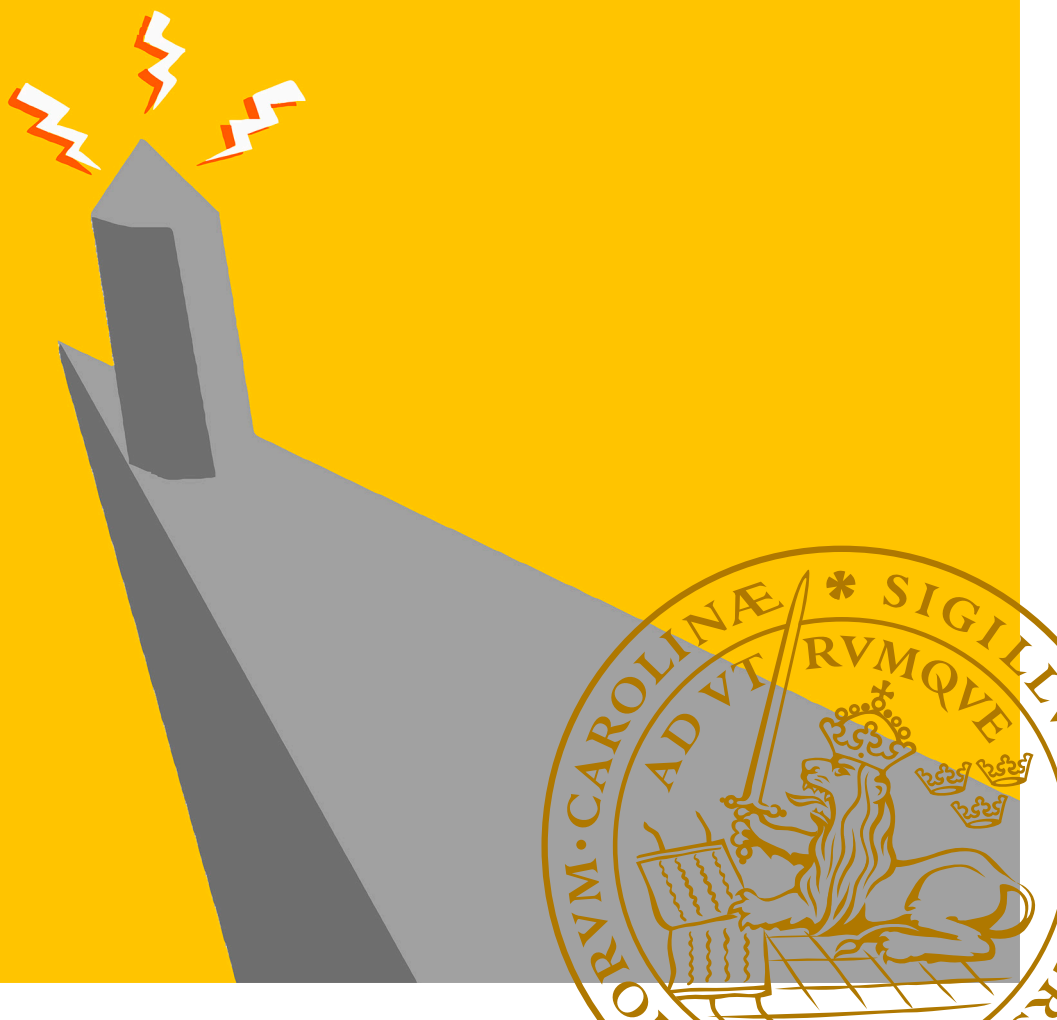

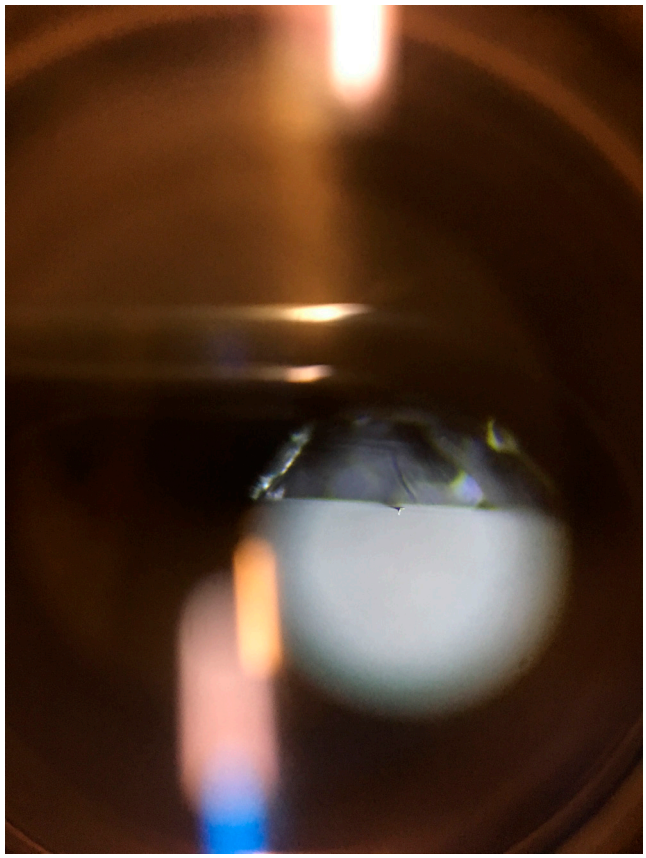

Even mobile phone cameras can take pictures of nanowires!

Printed by Media-Tryck, Lund 2019 NORDIC SWAN ECOLABEL 3041 0903

Lund University
Faculty of Science
Department of Physics
Division of Synchrotron Radiation Research
ISBN 978-91-7895-285-4

# Semiconductor Nanowires:

## Characterization and surface modification

Sofie Yngman

LUND
UNIVERSITY

DOCTORAL THESIS
by due permission of the Faculty of Science, Lund University, Sweden.
To be defended in the Rydberg Lecture Hall at the Department of Physics,
October 18, 2019, at 13.15.

*Faculty opponent:*
Prof. Karen Kavanagh
Simon Fraser University, Canada

| Organization | Document name |
|---|---|
| LUND UNIVERSITY | DOCTORAL THESIS |
| Division of Synchrotron Radiation Research<br>Department of Physics, Box 118, S-22100 Lund | Date of disputation<br>18 October 2019 |
| Author: Sofie Yngman | Sponsoring organization |


Title and subtitle:
Semiconductor Nanowires:
Characterization and surface modification


Abstract

The topic of III-V nanowires is still, after more than two decades, a growing and lively research area. The areas of application are wide and contain such important topics as energy harvesting, cheap and efficient lighting, high efficiency detectors and new types of electronics. III-V materials offer properties superior to the widely used Si. They can have considerably higher carrier mobility which paves the way for high-speed electronics and a great flexibility in band gap which is fundamental for optoelectronics. Producing these materials in the form of nanowires presents additional advantages as it gives the opportunity to tailor the material by altering the crystal structure and material composition in ways not possible in larger structures as well as integrating them with existing standard materials platforms.

This combination of great materials in a small size has demonstrated potential for improved solar cells, high-speed low power transistors as well as energy efficient and flexible LEDs. But the promises come with challenges. The quality of the III-V surfaces is a significant factor for determining device performance, potentially both improving and limiting functionality. Further, the relevance of surfaces properties increases with decreasing sizes as the surface to bulk ratio goes up. This thesis focuses on characterization of semiconducting III-V surfaces with a special focus on nanowires, exploring recently developed methods, types of nanowires and nanowire synthesis.

Native oxides forming on the surfaces of III-V materials in air are adverse and impede the development of top-tier devices. The surfaces have to be cleaned of the detrimental oxides and protected as part of the manufacturing of components. In the present work X-ray photoelectron spectroscopy (XPS) has been used to improve the understanding of different cleaning methods including the self-cleaning effect of atomic layer deposition (ALD) of high-k oxides.

Aerotaxy growth of nanostructures, where nanowires grow in a carrier gas, has arisen as a more cost effective and scalable production method than epitaxial growth on a solid substrate. Yet little is known about both the mechanism involved in the growth as well as about the quality of the resulting nanostructure surfaces. Here XPS and scanning probe microscopy (SPM) have been used to unravel the effect of doping on the surfaces of aerotaxy nanowires. Further, also a technique using small-angle X-ray scattering (SAXS) for in-situ characterization of the aerotaxy seed particles has been developed.

SPM has been a revolutionary tool for surface science since its invention. Central for the function of an SPM is the tip, which is usually made out of metal and formed by a simple electrochemical etching procedure. In this thesis the development of a high resolution GaN nanowire probe for SPM is described. It combines the optical and electronical advantages of GaN with the well-controlled tip formation at the end of a nanowire.



Key words
STM, AFM, XPS, semiconductor nanowires, high-k oxides, HP-XPS, SPM, SPM probes, H-cleaning, self-cleaning

Classification system and/or index terms (if any)

| Supplementary bibliographical information | | Language<br>English |
|---|---|---|
| ISSN and key title | | ISBN 978-91-7895-285-4 (print)<br>978-91-7895-284-7 (pdf) |
| Recipient's notes | Number of pages 215 | Price |
| | Security classification | |




Signature  Date 2019-09-09

# Semiconductor Nanowires

## Characterization and surface modification

Sofie Yngman


LUND
UNIVERSITY

*Front cover illustration by Johan Yngman:* An artistic visualization of a nanowire SPM probe.

*Back cover:* A photo of GaN nanowire on the tip of an AFM probe. The nanowire is reflecting light making it visible in a photo taken by a mobile phone through the ocular lens of an optical microscope.



Division of Synchrotron Radiation Research
Department of Physics
Lund University
SE-221 00, Lund
Sweden

ISBN 978-91-7895-285-4 (print)
ISBN 978-91-7895-284-7 (pdf)

Printed in Sweden by Media-Tryck, Lund University
Lund 2019


Media-Tryck is an environmentally certified and ISO 14001:2015 certified provider of printed material. Read more about our environmental work at www.mediatryck.lu.se

MADE IN SWEDEN

*To all of you non-physicists who still have the courage to pick up and read a PhD thesis.*

# Table of Contents

# Acknowledgement

To my supervisor Anders Mikkelsen, thank you for your optimism, support and for your trust in me. You provide a platform for your students where we are truly allowed to make cool things happen. I admire your way of accepting and embracing failures and disappointments and how you can turn everything into a great story. Meetings with you always leave me calm yet with a thousand new things to do. I cannot imagine a better boss.

To my co-supervisor and mentor, Rainer Timm, thank you so much for everything. Above all other tremendous traits of yours including but not limited to, warm hearted, hardworking, humorous and calm in every situation, I want to especially thank you for always being able to separate person from performance which ultimately creates an environment where people can fail, build confidence and finally perform well.

Chu Zhang, you have made my life richer and I have learned so much from you and our different perspectives. We have shared as many emotions as office days through the years.

Filip Lenrick, my companion, mentor and friend. Thank you for endless hours of GaN trippin'. Your knowledge of just about everything is astonishing. How?! I highly appreciate all your feedback on paper manuscripts and the manuscript of this thesis. Thank you also for creating "lunchklubben" which is also acknowledged for great lunches and discussions.

Andrea Troian, your active support during the writing of several papers and especially during the writing of this thesis has been invaluable to me. Your carefulness and exactness is only exceeded by your kindness and warmth. Thank you so much.

Patrik Wirgin, oh gosh, you should have an entire page for yourself. Thank you so much for all the support and encouragement you have given me through the years, both on work related matters and personal matters. I already miss you.

Edvin Lundgren is acknowledged for organizing the best kick-offs that any work place could wish for.

Achim Schnadt, you are my favorite person to disagree with which is a much fancier trait than it sounds like.

Johan Gustafson, your contagious laugh through the corridors can make any gray November day brighter.

Johan Knutsson, Olof Persson, Martin Hjort and Erik Mårsell. I didn't know what I had until you were gone from the division and you have been missed every step of the way since. Jesus, you guys are wild mad lads.

Huge thanks to Sara Blomberg, for laying the foundation of the pleasant working environment still present at sljus and to the rest of the division for maintaining it.

Sarah McKibbin and Estephania Lira, the mamas of the division! Thank you Sarah for all the aerotaxy shenanigans and thank you Estephania for always knowing the where's and what's in the labs.

Teaching has been a huge part of my time here at Sljus. Something I am truly grateful for. Even more grateful am I for being part of the splendid and outstanding team that has built up the course in Sustainable Development – Elisabeth Nilsson, Charlotta Nilsosn, Knut Deppert, Carina Fast and Erik Mårtensson. Elisabeth, Carina and Charlotta, you three together makes up for possibly a third of my collection of wise women (yup, I have a collection). You are inspiring and the ways you show guide me in several areas of life. Knut, you are also wise. Erik, we share some core values which are not always found at the university, thank you for that.

Life as a PhD student is filled with so much joy and fun challenges but it is rarely straight forward. During the years I have had the immense pleasure of being confided in by so many of you. I share or have shared, many of your feelings of doubt, self-criticism, despair, anger and tiredness. Every encounter has left me humbled and grateful for your trust. Rest assured that I believe in you and whatever choices you might make for the future.

Billions of outstanding nanowires have passed through the labs during my years here and not even one was grown by me. Thanks to a lot of people at the division of Solid State Physics, I want to especially thank Maryam Khalilian, Sebastian Lehman but also Jonas Ohlsson and Lars Samuelson.

I would also like to thank the splendid research group, with Lars-Erik Wernersson in the lead, at Electrical and information technology. The whole group sparks of optimism and generosity, it has been a great pleasure to collaborate with you.

Håkan is acknowledged for not only providing tools and nice chats but also for standing up for me, in a blink of an eye, whenever I needed it. To pass by your workshop is the only legit reason for me to walk indoors between the office and the labs.

The Santa Barbara crew is acknowledged as great karaoke partners and conference company.

I have also had the great pleasure of spending time at MAX IV, especially at MAXPEEM. Alexei Zakharov, you inspire! You also remind me of Daniel Day-Lewis which seems to be a truly great person, just like you.

During the years I have had the great pleasure to be accompanied by several hard working master and bachelor students; you have all contributed in different ways. I especially want to thank Saber Samadi. Your questions have kept me alert, your enthusiasm for the project and your hard work stretched far outside the scope of your own project.

**Janjoo** is acknowledged for housing me in Gävle, providing me with splendid bonus-colleagues and office space.

Thanks to Lisa and Camilla for keeping me insane.

To RUDE Boys; rum_h4m, Flinder, Ponny, kman, Wigman, Bullen, Phillan and Zeta. The first people I go to when I forget to save important data. Stay rude. I am not myself when I am not gaming.

Jacob Frödin, thank you for being the best possible father to our son Henry. Work is so much easier to focus on when I know that you two are in each other's splendid company. Also thank you for always believing in me and trying to facilitate everything work related, it means more than I can tell. Henry, I love you, you are the best thing I have made.

To my parents Karin and Michael Yngman, the most important ones, thank you for always believing in me and my dreams and for not making a difference whether the dreams are about horse racing, eSports or science.

To my sister Tilda and her Pontus and their lovely Elsie, for doubtlessly believing and endlessly supporting, thank you!

To my brother Johan, even in the darkest times you can dig up that inspiration and childlike curiosity that sometimes seems to lie buried too far away. That has been a huge asset in pursuing a PhD. You provided great support in the last stages of the writing of this book and you gave it the perfect front cover illustration. Also you can somehow always make me laugh. Thank you!

Johannes, thousands of miles in the train office and hundreds of quiet, focused hours by your side provided me with just the kind of an isolated bubble I needed to finish this book. I strive to match you in your ability to completely focus on a task at hands and to always choose the seemingly right way over the easy one. Your love makes me stronger, happier and prouder and I cannot wait for all the adventures that lie before us.

# Abstract

The topic of III-V nanowires is still, after more than two decades, a growing and lively research area. The areas of application are wide and contain such important topics as energy harvesting, cheap and efficient lighting, high efficiency detectors and new types of electronics. III-V materials offer properties superior to the widely used Si. They can have considerably higher carrier mobility which paves the way for high-speed electronics and a great flexibility in band gap which is fundamental for optoelectronics. Producing these materials in the form of nanowires presents additional advantages as it gives the opportunity to tailor the material by altering the crystal structure and material composition in ways not possible in larger structures as well as integrating them with existing standard materials platforms.

This combination of great materials in a small size has demonstrated potential for improved solar cells, high-speed low power transistors as well as energy efficient and flexible LEDs. But the promises come with challenges. The quality of the III-V surfaces is a significant factor for determining device performance, potentially both improving and limiting functionality. Further, the relevance of surfaces properties increases with decreasing sizes as the surface to bulk ratio goes up. This thesis focuses on characterization of semiconducting III-V surfaces with a special focus on nanowires, exploring recently developed methods, types of nanowires and nanowire synthesis.

Native oxides forming on the surfaces of III-V materials in air are adverse and impede the development of top-tier devices. The surfaces have to be cleaned of the detrimental oxides and protected as part of the manufacturing of components. In the present work X-ray photoelectron spectroscopy (XPS) has been used to improve the understanding of different cleaning methods including the self-cleaning effect of atomic layer deposition (ALD) of high-*k* oxides.

Aerotaxy growth of nanostructures, where nanowires grow in a carrier gas, has arisen as a more cost effective and scalable production method than epitaxial growth on a solid substrate. Yet little is known about both the mechanism involved in the growth as well as about the quality of the resulting nanostructure surfaces. Here XPS and scanning probe microscopy (SPM) have been used to unravel the effect of doping on the surfaces of aerotaxy nanowires. Further, also a technique using small-angle X-ray scattering (SAXS) for *in-situ* characterization of the aerotaxy seed particles has been developed.

SPM has been a revolutionary tool for surface science since its invention. Central for the function of an SPM is the tip, which is usually made out of metal and formed by a simple electrochemical etching procedure. In this thesis the development of a high resolution GaN nanowire probe for SPM is described. It

combines the optical and electronical advantages of GaN with the well-controlled tip formation at the end of a nanowire.

# Populärvetenskaplig sammanfattning

Först halvledarteknik, sedan nanoteknik. Tillsammans utgör de huvuddelen av det vi definierar som modern teknik. Användandet av halvledare revolutionerade teknologin under mitten av 1900-talet genom möjligheten att kunna kontrollera halvledarmaterial till att vara antingen elektriskt isolerande eller ledande. Inom elektroniken utgör halvledarna den viktigaste beståndsdelen i till exempel datorer, lysdioder och solceller. En modern värld utan halvledarteknik är mycket svår att föreställa sig.

Nanoteknik beskriver teknik med komponenter i nanostorlek. En nanometer är 0.000000001 m, alltså en miljondel av en millimeter. För att få perspektiv så kan man föreställa sig att klyva ett typiskt människohår hundratusen gånger för att få ner tjockleken till en nanometer. Nanoteknik används inom flera stora områden såsom biologi, medicin, kemi och fysik och vi stöter på den dagligen i exempelvis våra mobiltelefoner.

**U**nder de senaste decennierna har nanotekniken utvecklats från att vara en framtida vision till en högst verklig nutid. Det finns gott om plats på botten (”There’s plenty of room at the bottom”), är den berömda titeln på Richard Feynamns föreläsning från december 1959 där han förutsåg nanoteknologin och manipulation av atomer. Idag, nära 60 år senare, är sanningen den att vi början få slut på utrymme.

Inom elektroniken talar man ofta om storleken på transistorer och hur många transistorer som får plats på ett litet utrymme. Utvecklingen har under flera decennier följt Moors lag som ungefär säger att antalet transistorer som får plats på ett chip fördubblas vartannat år. Snart har vi nått gränsen för att transistorerna inte längre kan skalas ner i storlek utan att kvantmekaniska effekter börjar blanda sig i.

När vi skalar ner storleken på föremål till en punkt där föremålet är i storleksordningen av atomer så spelar ytor en väldigt stor roll. Antalet ytatomer utgör då plötsligt en väldigt stor andel av hela föremålet. En parallell skulle kunna vara att tänka på färgen hos en tusensköna. Jag slår vad om att du tänker på vitt trots att mitten hos blomman är gul. De vita kronbladen är våra ytatomer och den gula mitten är insidan av våra nanomaterial. Samspelet mellan ytatomerna och dess omgivning blir plötsligt det som definierar föremålets egenskaper. Hade de vita kronbladen hos tusenskönan ramat in ett föremål stort som solen så hade vi säkerligen ändå definierat solen som gul. Den ringa storleken på objekten gör alltså att ytor och de yttersta lagren av atomer spelar en stor och viktig roll inom nanotekniken.

Kisel är halvledarmaterialet som bygger upp mer eller mindre alla halvledarkomponenter i dagens elektronik. En fantastisk fördel med kisel har varit

just dess ytor som med nästan ingen modifikation varit nära nog perfekta. Kisel har dessutom varit billigt och lättillgängligt men nu behöver vi titta på alternativa material för att på andra sätt fortsätta utvecklingen. Ytterligare en formulering av Moors lag uttrycker att beräkningskraften fördubblas vartannat år. Det öppnar för möjligheten att, istället för att minska storleken, byta ut materialen i transistorerna till material med högre ledningsförmåga för att öka hastigheten i komponenterna och därmed beräkningskraften.

III-V-halvledare består av föreningar av element från tredje och femte gruppen i periodiska systemet. Sådana föreningar, tex galliumarsenid, indiumarsenid, indiumfosfid och galliumnitrid har betydligt högre ledningsförmåga än kisel och skulle kunna utgöra en viktig del i höghastighetselektronik. Ett problem med dessa material har dock varit att deras ytor och gränsskikt haft många defekter vilket har hämmat prestationen hos sådana komponenter.

I den här avhandlingen studeras nanostrukturer i form av III-V nanotrådar. Nanotrådar är små, stavliknande strukturer med diameter i nanostorlek (20-400 nm) och längd i mikrometerstorlek (1-10 μm). Själva formen bidrar med flera fördelar jämfört med att ha materialet i stor, bulkform. Dels så uppstår färre deformationer när man tillverkar (växer) materialet i trådform än på stora ytor, dels är laddningstransport i nanotrådar effektivare. Det gör III-V nanotrådar till ett flexibelt material med många tillämpningsområden inom elektronik.

Den här avhandlingen beskriver framsteg inom framförallt tre olika fält av nanotrådsforskning nämligen ytförbättring, växt och applikationer.

Först undersöks metoder för att förbättra kvaliteten hos ytor både på nanotrådar och på större platta material. Framförallt beskrivs hur man med hjälp av röntgenljus kan undersöka hur ytorna kan förbättras genom rengöring och kontrollerad lager-på-lager-växt av oxider.

Dessutom studeras den nya, revolutionerande växttekniken aerotaxi. Genom aerotaxi så kan nanostrukturer produceras både billigare och snabbare än via traditionella växttekniker. Dock behöver vi fortfarande lära oss mer både om fysiken bakom den nya växtmetoden och om resultatet av nanostrukturer växta med den. Här beskrivs ett sätt att undersöka själva växtmetoden.

Till sist beskrivs hur nanotrådar även kan användas som ett nytt verktyg inom svepprobsmikroskopi och svepprobsspektroskopi genom att utnyttja den stora kunskapen om hur nanotrådarna ser ut och beter sig. Det öppnar för användandet av nanotrådar för vidare ytkaraktärisering på atomnivå av nanoobjekt där just svepprobmikroskopi varit den ledande tekniken.

# Abbreviations and symbols

| | |
|---|---|
| 1D, 2D, 3D | One-, two-, and three-dimensional |
| $\Phi$ | Work function |
| $\psi$ | Wave function |
| $E_B$ | Binding energy |
| $E_F$ | Fermi level |
| $E_k$ | Kinetic energy |
| $E_{VAC}$ | Vacuum level |
| $hv$ | Photon energy |
| $I_T$ | Tunneling current |
| $V_T$ | Tunneling voltage |
| III-V | Compound consisting of a group III and a group V element from the periodic table. |
| AFM | Atomic force microscopy |
| ALD | Atomic layer deposition |
| BG | Band gap |
| CB | Conduction band |
| EBID | Electron beam deposition |
| FIB | Focused ion beam |
| HP-XPS | High-pressure X-ray photoelectron spectroscopy |
| IMFP | Inelastic mean free path |
| (L)DOS | (Local) Density of states |
| LED | Light emitting diode |
| MBE | Molecular beam epitaxy |
| MOSFET | Metal oxide semiconductor field effect transistor |
| MOVPE | Metal organic vapor phase epitaxy |
| NW | Nanowire |
| SEM | Scanning electron microscopy |

| | |
|---|---|
| SPM | Scanning probe microscopy |
| STM | Scanning tunneling microscopy |
| STS | Scanning tunneling spectroscopy |
| TDMA-Hf | Tetrakis-dimethylamino hafnium |
| TEM | Transmission electron microscopy |
| TIBB | Tip-induced band bending |
| UHV | Ultra-high vacuum |
| VB | Valence band |

# List of papers

In this thesis the following papers are included.

I

**Surface smoothing and native oxide suppression on Zn doped aerotaxy GaAs nanowires**

*S. Yngman, S. R. McKibbin, J. V. Knutsson, A. Troian, F. Yang, M. H. Magnusson, L. Samuelson, R. Timm, and A. Mikkelsen*

Journal of Applied Physics **125**, 025303 (2019)

In this paper we present the effect of Zn doping on aerotaxy grown GaAs nanowires. We compare nanowires exposed to different amount of Zn present during growth. Using synchrotron radiation based XPS we find that a high nominal doping reduce the formation of native oxides on the nanowire surfaces. From AFM measurements we learn that a high doping also smoothens the nanowire surface morphology. The smoothing in combination with the reduced amount of native oxides and a thorough investigation of the XPS data at different photon energies, leads us to conclude that the high amount of Zn during growth results in a protective ZnO shell.

*I took part in the planning of the experiment and the XPS measurements. I was responsible for the AFM measurements, the data analysis and I was the main responsible for writing the paper.*

II

**GaN Nanowires as Probes for High Resolution Atomic Force and Scanning Tunneling Microscopy**

*S. Yngman, F. Lenrick, Y-P. Liu, Z. Ren, M. Khalilian, B. J. Ohlsson, D. Hessman, L. Samuelson, R. Timm, and A. Mikkelsen*

Submitted (2019)

In this paper we present the first STM measurements with a single GaN nanowire probe. We describe a fabrication method where we use a nanomanipulator inside an SEM to place single nanowires on the tip of SPM probes. We show results from AFM, STM and STS measurements with such probes on various surfaces, metallic as well as semiconducting. We also discuss how the probes can be further developed to function also for other SPM techniques such as SNOM and STL.

*I was one of the responsible for the planning of the experiment and I was the main responsible for the measurements, the data analysis and for writing the paper.*

III

**Characterization of GaSb surfaces and nanowires during oxide removal**

*S. Yngman, G. D'Acunto, Y-P. Liu, A. Troian, A. Jönsson, J. Svensson, L-E. Wernersson, A. Mikkelsen and R. Timm*

In manuscript (2019)

In this paper we present a detailed description of the cleaning of GaSb surfaces, both for planar substrates and nanowires. By the use of H-plasma cleaning we successfully remove the Sb native oxides as well as most of the tough Ga native oxides from the planar surfaces and nanowires. Remarkably, the removal of the oxides on nanowires is even more profound than on the planar substrate and continuous cleaning led to complete removal of all oxides except for only a small amount of $Ga_2O$ which is the least detrimental Ga-oxide.

*I was responsible for preparing the samples and the data analysis, I took part in planning and performing the experiment, and I was the main responsible for writing the manuscript.*

IV

**InAs-oxide interface composition and stability upon thermal oxidation and high-k atomic layer deposition**

*A. Troian , J. V. Knutsson, S. R. McKibbin, S. Yngman , A. S. Babadi, L-E. Wernersson, A. Mikkelsen, and R. Timm*

AIP Advances **8**, 125227 (2018)

In this paper we present synchrotron radiation based XPS measurements as well as STM and LEED experiments leading to a detailed description of the interface between InAs, a thermal oxide and an ALD high-k layer. We remove the native oxides by annealing in the presence of atomic hydrogen and replace these oxides by a well-controlled but non-crystalline thermal oxide. We find that the thermal oxide, though not stable to further oxidation in ambient conditions, leads to an interface with fewer defects which would improve device performance.

*I took part of the XPS measurements and discussion about the data analysis and contributed to discussions on the manuscript.*

V

**Self-cleaning and surface chemical reactions during hafnium dioxide atomic layer deposition on indium arsenide**

*R. Timm, A. R. Head, S. Yngman, J. V. Knutsson, M. Hjort, S. R. McKibbin, A. Troian, O. Persson, S. Urpelainen, J. Knudsen, J. Schnadt, and A. Mikkelsen*

Nature Communications **9**, 1412, (2018)

In this paper we present the first time resolved high pressure XPS measurements of the chemical reactions between InAs and the first cycle of ALD of $HfO_2$. Rather surprisingly we find that the self-cleaning process and hence the quality of the semiconductor-oxide interface is not, as earlier believed, controlled by the oxide formation but rather the molecular adsorption process that happens right before. This finding meant that the model of the ALD ligand exchange, that described the removal of the native oxides and the formation of the first ALD layer, had to be revised.

*I took part of the measurements and the data analysis of this paper and contributed to discussions on the manuscript.*

VI

**In situ observation of synthesized nanoparticles in ultra-dilute aerosols via X-ray scattering**

*S. R. McKibbin, S. Yngman, O. Balmes, B. O. Meuller, S. Tågerud, M. E. Messing, G. Portale, M. Sztucki, K. Deppert, L. Samuelson, M. H. Magnusson, E. Lundgren, and A. Mikkelsen*

Nano Research **12**, 25, (2019)

In this paper we present the first measurements of an extremely diluted aerosol using high-intensity synchrotron SAXS. The use of a Au aerosol for aerotaxy growth of nanowires has proven extremely effective. With careful consideration of the background removal we manage to study a low particle density stream with Au particles which is the first processing step in the aerotaxy growth. Using the same technique further down the processing line would allow for a detailed examination of the aerotaxy growth, something that is still lacking.

*I took part of the planning of the experiment and developing the measurement set-up. I was one of the responsible for the measurements and contributed to discussions on the manuscript.*

**The following papers are not included in this thesis.**

VII

**Structural Properties of Wurtzite InP-InGaAs Nanowire Core-shell Heterostructures**

*M. Heurlin, T. Stankevič, S. Mickevičius, S. Yngman, D. Lindgren, A. Mikkelsen, R. Feidenhans'l, M. T. Borgström, and L. Samuelson*

Nano Letters **15**, 2462, (2015)

In this paper we investigate the structural, compositional and optical properties of InP−InGaAs nanowires.

VIII

**Low Trap Density in InAs-High-k Nanowire Gate Stacks with Optimized Growth and Doping Conditions**

*J. Wu, A. S. Babadi, D. Jacobsson, J. Colvin, S. Yngman, R. Timm, E. Lind, and L-E. Wernersson*

Nano Letters **16**, 2418, (2016)

In this paper we present a detailed study on vertical wrap-gated InAs/high-k nanowire MOS capacitors.

IX

**In vivo detection and absolute quantification of a secreted bacterial factor from skin using molecular imprinted polymers in a surface plasmon resonance biosensor for improved diagnostic abilities.**

*G. E. Bergdahl, T. Andersson, M. Allhorn, S. Yngman, R. Timm, R. Lood*

ACS Sensors **4**, 717, (2019).

In this paper we developed a biosensor for detecting a bacterial protein that is an early indicator for some skin diseases.

# 1. Introduction

III-V semiconducting nanowires have been a topic of study for more than 20 years and it is still a vibrant area of research. III-V nanostructures in general have the advantage of offering different physical properties and technological advantages compared to bulk materials - that mainly arise from their size. With the reduction in size comes a high surface to bulk ratio compared to macro-scale which is presenting new opportunities and challenges. This type of structure can have a very wide variety of applications for both fundamental studies[1,2] and implementations in for example energy harvesting devices, such as solar cells[3,4], energy saving devices such as light emitting diodes (LEDs)[5,6] or in faster and more energy efficient computer chips[7]. However, the surfaces can also lead to additional losses in devices and in other ways affect function in a bad way which must also be understood and controlled.

Even if the research area of III-V nanowires has matured considerably, new opportunities and questions open up all the time as new types of nanowires[8] and growth methods[9,10] become available. With the present knowledge it is possible to enter the area of III-V semiconducting nanowires from different new directions such as using knowledge as input for special in-situ methods or using the nanowires as novel probe tools themselves. In the present study we utilize the impact of previous work as we explore interesting opportunities or questions created by recent III-V nanowire developments.

Several criteria have to be fulfilled for any nanostructure to be useful both for basic research and/or in real life applications. The present work touch upon three fundamentally important questions which need exploration to make any type of nanostructure viable for applications in science and technology, namely: How does it grow? How does it interact with the environment? What can it be used for?

The growth of nanostructures is a well-developed field with a lot of different options and opportunities including both bottom-up and top-down approaches[11]. In top-down approaches a larger piece of material is reduced in size by for example etching or ion milling[12]. In bottom-up approaches growth material from a supply is transitioned into a solid phase. Typically the supply is in gas form, but historically it was in liquid form[13]. III-V nanowire synthesis has often been performed bottom-up on a solid substrate using Au seed particles that promote growth underneath them thus creating a 1D nanowire. One new approach for growing III-V

semiconducting nanowires is aerotaxy growth in which Au seed particles flow freely in a gas but still initiate nanowire growth. Aerotaxy growth is potentially revolutionary as the growth time and cost is considerably cut due to the lack of expensive crystal growth substrates[14]. Therefore, the study of nanostructures grown with this technique is highly relevant. In this thesis both post growth studies as well as attempts to study the seed particles in-situ are presented.

Generally the growth of nanostructures is conducted in a well-controlled environment. To make devices out of grown nanostructures, or to transport them, the nanostructures often need to be taken out of their initial growth environment, something that imposes reactions such as oxidation to the nanostructure surface. The reactions to different environments are explored in experiments presented in this thesis where the native oxides are being removed and new oxides added in a controlled fashion. The controlled reduction and formation of high quality surface oxides are crucial in order to develop high quality devices that can function also for example in air. In atomic layer deposition growth material is supplied in gas form to a substrate resulting in the controlled deposition of single atomic layers of material. Atomic layer deposition of insulating layers of oxides is now one of the standard techniques for achieving high quality surfaces and interfaces[15]. The ALD process has been studied *in-situ* using X-ray Photoelectron Spectroscopy (XPS).

The use of nanostructures is not limited to (opto)electronics, even if this is a huge field of research, but they can also be used as tools to, for example, interact with living cells[16] or probe inside the brain[17]. Anywhere were nano sized structures are found there might be a need for a nano-tool to characterize them. In this thesis a novel example of such a nano-tool is presented as the development of a special nano-probe for scanning probe applications is described. Single GaN nanowires are placed onto probes for Scanning Probe Microscopy (SPM). The high hardness of the semiconducting GaN in combination with the well-known shape of nanowires is advantageous for SPM. The shift from the commonly used metal probes to semiconducting probes offers interesting possibilities of surface studies of for example electronic properties.

In the end it boils down to a focus III-V nanowire characterization, both exploring new methods for looking at and with them as well as working on how to control in particular the surface oxides on the nanowires which has turned out to be crucial for their functionality.

This thesis is divided into two main parts. In the first part you can find a series of chapters giving an introduction and a context to the second part which is a collection of scientific papers. In the chapters in the first part I aim to give a broader background to the scientific papers to make them available for a more general public outside the specific fields.

In **Chapter 2** I introduce the fundamental concepts of semiconductors, nanowires and especially III-V semiconducting materials. The focus is on the surfaces and the surface oxides of these materials.

In **Chapter 3** I present the methods that have been used to characterize surfaces and nanowires. I describe the concepts of Scanning Tunneling Microscopy and Atomic Force Microscopy (AFM) that has been used both for characterization of nanowires and for characterization with nanowires. I also give an introduction to XPS and how we use it as a tool to map surface oxides. Finally Small Angle X-ray Scattering (SAXS) is briefly discussed.

In **Chapter 4** there is a more detailed description of how we characterize surfaces of nanowires. I describe our work with characterizing the surfaces and interfaces between III-V semiconductors and high permittivity oxides. I give details about the surface of doped GaAs aerotaxy nanowires and talk about how we have developed techniques for further characterization of aerotaxy growth. Finally, I describe our development of GaN nanowires as promising probes for SPM.

In the beginning of each chapter and whenever relevant I refer to the papers in the second part of the thesis by their roman numerals.

# 2. Semiconducting III-V surfaces and nanowires

In this chapter I describe the fundamentals of semiconductors, especially III-V semiconducting nanowires. Semiconductors are part of nearly all experiments included in this thesis and can be found in each of the **papers I-V**. Additionally, the Au particles in **paper VI** work as the seed particles for growing semiconducting nanowires. I introduce concepts such as doping, band structure and band gap that define the electronic properties of a semiconductor and talk about the relevance of surfaces for devices. I finally describe the basics of nanowires, how they are grown, tailor made for different purposes and oxidized and cleaned.

A world without semiconductors would be unrecognizable to most of us. Without semiconductors we would have no digital computers or cell phones. Historically the most used semiconductor material is Si. Although Ge was the first material to be used frequently in semiconductor industry in the early 20$^{th}$ century, soon the superior electrical properties and the advantageous formation of $SiO_2$ (and also price and availability) of Si pushed Ge out to the periphery[18]. Still, the demand for faster, smaller and more versatile electronics increases every year and with that the need for materials to meet those demands.

Semiconductors are insulators with a small band gap. There is no exact definition of this "small" size of the band gap, but material scientists often denote a material as semiconducting if its electrical conductivity at a high temperature is as good as for a metal but nearly absent at low temperatures[19]. The electronic properties, or more specific the number of charge carriers of a semiconducting material can be altered in a controllable way by introducing impurities, a process called doping. This possibility to change the electrical properties of the semiconductor in a controllable manner has made it a versatile and useful tool in electronics. In Figure

2.1 the difference in band structure between a metal, a semiconductor and an insulator is shown. At room temperature a semiconductor is a better conductor than an insulator, but not as good a conductor as a metal. With added energy, for example by shining light on, or heating up, the material, the electrons in the valence band can be excited into the conduction band and leave holes in the valence band as depicted in Figure 2.1 (b). For semiconductors the added energy arising solely from the material being at room temperature is enough to excite some electrons and make the material weakly conductive. For an insulator a much higher energy is needed to excite the electrons across the band gap.

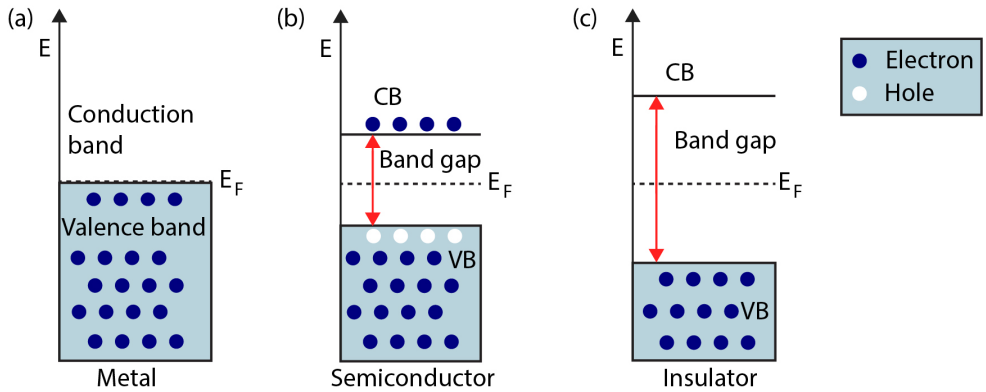


**FIGURE 2.1**
Schematic illustration of the band structure of (a) a metal, (b) a semiconductor and (c) an insulator. The Fermi level is denoted as $E_F$ and the band gap is indicated by red arrows. The position of the conduction band (CB) and the valence band (VB) are also indicated in each case.

## 2.1. III-V materials

Both Si and Ge belong to group IV of the periodic table. Another class of materials is III-V semiconductors. They are compounds made up of elements from group III (e.g. group 13 including B, Al, Ga, In, Tl) and group V (e.g. group 15 including N, P, As, Sb, Bi). In these two groups we find post-transition metals, metalloids and reactive non-metals.

There are several inherent properties of semiconducting materials that differ depending on the elements present in the material. Some of these properties are; band gap size (and if the band gap is *direct* or *indirect*), carrier mobility and carrier generation and recombination. Such properties are tailored as we explore new combinations of elements. The compounds constituting the III-V group of materials show great promise in offering semiconductors with direct and variable bandgaps as well as higher carrier mobility than that of the widely used Si[20]. The

III-V semiconductors can also be altered to have an excess of either electrons or holes via doping and the resulting semiconductor is denoted *p*-type (positive-type, excess of holes) or *n*-type (negative-type, excess of electrons). However, combining materials into new ones is not trivial as the crystal lattices between the materials have to match in order to avoid harmful dislocations and strain. Growing the material into nanostructures such as nanowires can act as a way of avoiding that issue[21].

In this section I will now describe doping, how it affects the band structure and band gap of the material, I will talk about the relevance of surfaces and finally give some example of devices and what they are used for.

### 2.1.1. Doping

The III-V materials can be doped to have an excess of electrons, called negatively doped or *n*-doped, or an excess of holes, called positively doped or *p*-doped. For doping of III-V materials group II atoms (e.g. Zn) are often used for *p*-doping where their substitution contributes with an additional hole. Furthermore, group VI atoms (e.g. Sn) are often used for *n*-doping where they contribute with an extra (free) electron. Dopants can be introduced during the growth of the material, or afterwards via diffusion[19] or ion implantation[22]. If a semiconductor is grown without any intentional added dopants it is said to be nominally undoped or intrinsically doped since a small amount of impurities always will be present.

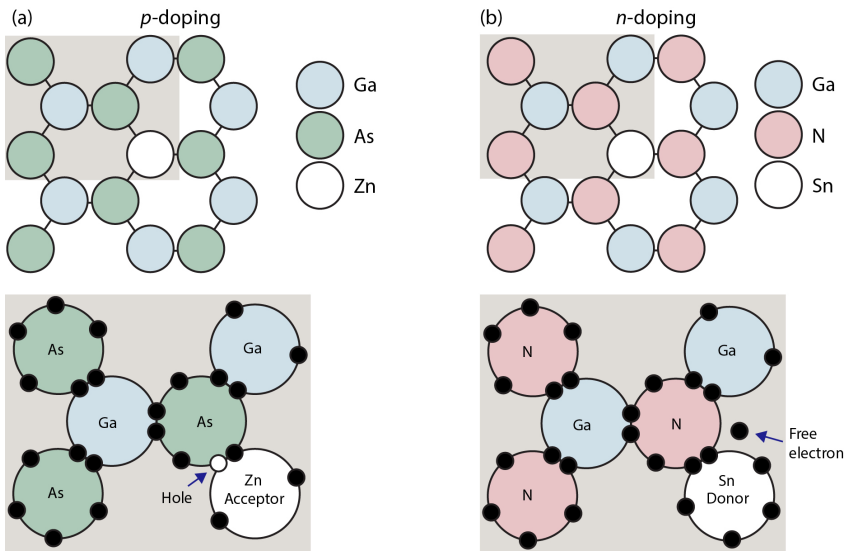


**FIGURE 2.2**
Schematic illustration of (a) by Zn *p*-doped GaAs and (b) by Sn *n*-doped GaN. The circles represent the atoms and the black dots on the circles represent the valence electrons.

An *n*-doped material has an excess of electrons in the conduction band at room temperature. A minute amount of the atoms in the bulk material has been exchanged to atoms with a larger number of valence electrons. The atoms with the extra valence electrons are called *donors*. Similarly a *p*-doped material has an excess of holes. The added dopants in a *p*-doped material have less valence electrons than the bulk material and are called *acceptors*. In Figure 2.2 schematic illustrations of a material that is (a) *n*-doped and (b) *p*-doped are shown. In this work I have often used GaAs aerotaxy nanowires *p*-doped with Zn and GaN nanowires *n*-doped with Si.

Measuring dopants in a material is crucial but not always straightforward and a lot of efforts are directed towards addressing this challenge[23] this is especially an issue for nanostructures, due to their small size.

### 2.1.2. Band structure and band gap

The doping of a material alters the position of the Fermi level of the material. For a metal, the Fermi level is defined, at 0 K, as the highest energy to which available states are filled with electrons. Above the Fermi level only empty states exist. For a semiconductor it is more correct to talk about the chemical potential of the electrons. We often, a bit carelessly, denote it Fermi level also for semiconductors and I will do so throughout the text. For an intrinsically doped (undoped) material at 0 K the Fermi level is found close to the middle of the band gap of the semiconductor. But this is not always the case as described in Figure 2.3.

There are several reasons to why the Fermi level is not always in the middle of the semiconductor band gap. The Fermi level will shift towards the band with lowest effective mass of electrons (or holes). When a semiconductor is doped, with added impurities, this balance change, and the Fermi level shifts. The system will counter the added impurities to stay at equilibrium by shifting the Fermi level towards the conduction band or the valence band depending on the type of dopants. If the material is *n*-doped, and hence has an excess of electrons, the Fermi level will move towards the conduction band and vice versa for a *p*-doped semiconductor.

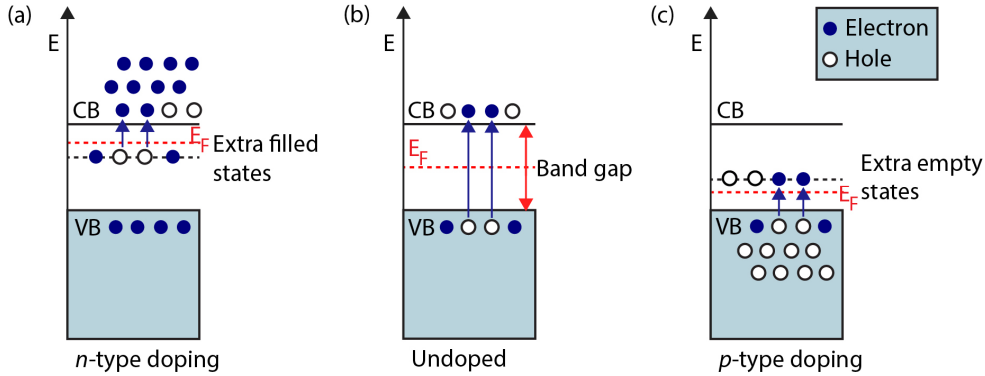


**FIGURE 2.3**
Schematic illustration of (a) *n*-type doping, (b) intrinsic doping and (c) *p*-type doping. The red arrow indicate the size of the band gap. In the case of *n*-doping, where the dopants contribute with extra electrons, these extra electrons will act as free electrons as they get excited into the conduction band and hence boost the electron conductivity of the material. In the case of *p*-doping the situation is reversed and the dopants will instead contribute with extra holes in the valence band.

In the band gap of a semiconducting bulk material at room temperature the doping levels will typically have donated all their carriers to the conduction/valence band and thus no further states or no states are available. But there are several things that can induce states in the band gap or bend the bands close to the semiconductor surface. Two examples, relevant for the studies in this thesis but quite different from each other, are surface states and tip induced band bending.

Surface states are induced at the surface as the bulk is suddenly truncated. The atoms at the surface that normally would bind to the next layer of atoms will find themselves missing some nearest neighbours and thus left with dangling bonds. The net charge of the surface must be neutral meaning that if such surface states are charged (they can be neutral, positively charged or negatively charged) a surface band bending will be induced to reach neutrality again[24].

An STM probe itself may bend the onset of the bands because it applies a voltage potential between the tip and the surface. This is called tip induced band bending and is explained in section 3.1.3. Other states that are often found in the band gap are defect states[25], induced by defects in the crystal.

### 2.1.3. Surfaces and interfaces of III-V materials

The importance of the surface of a device increase as the size of the device decreases. At a nanoscale, where the ratio of surface to bulk material is high, the physical properties at the surface therefore often dictate the properties of the entire device. In addition, it is important to note that the surface is the region where a

material interacts with its surroundings making it a crucial part of all electronic devices.

As most materials, the III-V surfaces usually oxidize when exposed to ambient conditions. The resulting oxides depend on the compound materials, but usually the oxides are un-ordered and with a thickness of 1-2 nm[26,27]. To achieve a functioning device these native oxides often need to be removed and replaced with a well-controlled high-*k* oxide through e.g. Atomic Layer Deposition. Other techniques exist, such as passivation through chemical etching, protecting capping layers or $SiO_X$ deposition, to maintain a good enough surface quality[28]. However, there are significant differences between the surface properties of III-Vs. For example for InP solar cells, it is possible to keep the oxide since the surface quality is high enough making the recombination velocity in InP low[29]. Also from an STM point of view the native oxides are detrimental since they are not only insulating but also cover the interesting surface below.

Thanks to the development of techniques to deposit atomic layers of materials it is now possible to tailor suitable mixes of semiconducting materials and oxides. Atomic Layer Deposition (ALD) gives exactly this opportunity (explained in section 2.2.3). A lot of effort has been put into finding which materials to use as high performing oxide layers in devices. The ALD of some specific oxides on III-Vs functions also as a passivation layer of the semiconductor surface. We have studied the effect and process of ALD of $HfO_2$ and $Al_2O_3$ on InAs in detail and in section 4.1.1 I give an overview of these studies.

### 2.1.4. Devices

A variety of (opto)electronic devices are produced from semiconductors; Light emitting Diodes (LEDs), Laser diodes, Field-effect transistors (FETs) and solar cells are just a few examples[19].

The Metal-Oxide-Semiconductor Field-effect Transistor (MOSFET) is an electronic device that has revolutionised electronics since its invention in the 50s. It can now be found in basically all electronics that we use and are produced in billions every day.

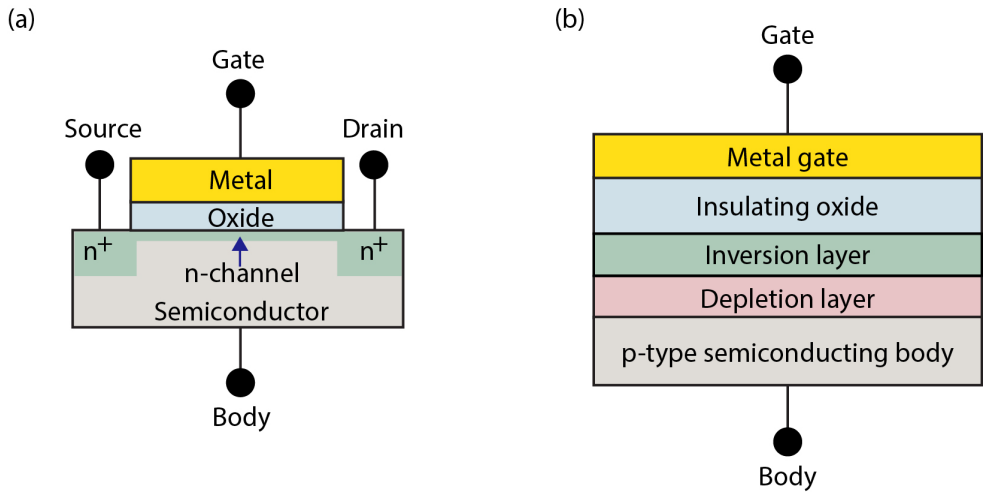


**FIGURE 2.4**
Schematic illustration of (a) a MOSFET with indications of the four terminals; source, drain, gate and body. (b) shows a gate stack with its many interfaces.

The MOSFET is a field effect transistor consisting of layers of a metal, an oxide and a semiconductor as depicted in Figure 2.4. The MOSFET consists of a semiconducting body with a channel connecting a source terminal to a drain terminal. The conductivity of the channel can be controlled via a voltage applied over the gate and the body of the transistor. The metal gate is isolated from the semiconducting source and drain (assumed to be *n*-type here) by an insulating oxide layer.

The channel arises as the voltage applied to the gate modifies the distribution of charges in the semiconductor. If no voltage is applied over the gate and the body the resistance will be very high as each of the terminals in the body presents a *pn*-junction. A positive voltage applied to the gate will push away the positive charges (holes) close to the semiconductor-oxide interface and a depletion region will occur. If the voltage is high enough to push away enough holes to make electrons the majority carriers there will be a region with an *n*-type channel close to the interface connecting the *n*-type source and drain. If a voltage is then applied over the source and the drain a current will flow through the channel and the transistor is in an ON state.

For device performance an oxide with high permittivity is desirable. The permittivity determines a materials ability to store an electric field. We usually talk about high-*k* oxides or materials with a high *dielectric constant* which is the ratio of a materials permittivity over the permittivity of free space.

The MOSFET contains several interfaces (Figure 2.4 (b)). The structural quality of the interfaces directly influences the conductivity and device performance. During device fabrication unwanted atomic scale defects are introduced. One such defect is oxides resulting in high interface trap densities. This is explored in section 4.1 as we look closer on surface oxidation and ALD to reduce native oxides.

### 2.1.5. Surface cleaning

One common approach to clean semiconducting surfaces of their native oxides is by annealing in ultra-high vacuum (UHV). The sample is heated and oxides and surface contaminates are desorbed from the surface. This works well for many large structures and substrates, but impose a problem for most III-V materials and especially nanowires that due to their structure and small size risk decomposing before cleaning temperatures have been reached. However, there are alternatives allowing cleaning at lower temperatures. In this work mainly cleaning with atomic hydrogen has been used, but also, in **paper III**, hydrogen plasma cleaning was used.

#### *Atomic hydrogen cleaning*

A flow of hydrogen passes a heated W-filament with a temperature of above 1700°C. The high thermal energy supplied by the filament cracks the hydrogen molecules into atomic hydrogen. The atomic hydrogen is extremely reactive and reacts with the native oxides on the surface and the resulting products are thought to be more volatile and therefore desorbs at lower temperature[30]. Common cleaning temperature of III-V surfaces and nanowires using H-cleaning is between 300°C and 600°C depending on the material[31].

Since the hydrogen radicals have a very low kinetic energy, in the order of 1 eV, the interaction between the sample and the hydrogen is limited to the sample surface. After cleaning and the shutdown of the hydrogen supply the surface is kept at high temperature for a few minutes to desorb any redundant hydrogen.

#### *Hydrogen plasma cleaning*

Instead of atomic hydrogen cleaning a hydrogen plasma can be generated and used as was done in **paper III**. An artificial plasma can be generated using a Tectra gen 2 plasma source which generate the plasma by the use of wave coupling of microwaves[32]. Hydrogen plasma cleaning has been proven effective before on both GaSb[33] as well as InGaAs[34].

## 2.2. III-V nanowires

The development of nanowires arises from a fundamental curiosity of physical dimensions and what happens when these are reduced. New applications were also envisioned early on as it was possible to combine different III-Vs in new ways as one did not have to take strain into account[35]. Nanowires also offer great flexibility in design as it is possible to change III-V material and doping during growth just by switching the growth precursors.

The field of nanowire research was small until the very beginning of the 21st century when it exploded and has since then experienced an almost exponential increase in interest (measured by the use of the word "nanowire(s)" in scientific publications)[36]. Even so, the first reports on semiconducting nanowires date back to 1957[37].

Nanowires are rod shaped nanostructures. Their dimensions vary greatly depending of area of application and use and desired properties. The nanowire dimensions allow a potential well to be formed by the boundaries of the nanowires. Therefore nanowires can often be considered a 1D material where the electrons are confined to travel along the axis of the nanowire.

Due to their structure nanowires have a huge surface to bulk area. Much of the properties of the nanowires are consequently dependent on the quality of the surface of the nanowire. For III-V nanowires the surface or interface between the semiconductor and its oxide can be problematic. The III-V surfaces still struggle with a higher defect density than for example Si and $SiO_X$. Defects arise partly from surface states positioned in the band gap of the semiconductor. Some surface states arise from the breaking of the bulk symmetry, as discussed in section 2.1.2. Other surface states are instead an effect of defects at the surface or interface. If the surface states are positioned inside the band gap of the semiconductor they will induce band bending and Fermi level pinning resulting in that the Fermi level can no longer be controlled by an external bias but is only an effect of the donor like or acceptor like state of the defects.

The III-V nanowires are not only promising because of their high carrier mobility, from an electronics point of view they are especially interesting as they can be grown onto Si surfaces allowing an integration onto the main chip technology platform used presently[38,39,40]. However, some applications (such as solar panel arrays) have large demands on the amounts of III-V nanowires needed which has been a challenge to meet as the number of ordinary epitaxial growth of nanowires is limited by its expensive and small growth substrates. To meet this demand the new growth technique aerotaxy has recently emerged as a viable alternative which is both cheaper and faster, but the growth process is to a large extent unexplored. We have examined some of the nanostructures grown by the technique and we

have also developed means of further exploring the growth process *in-situ*. This is described in section 4.2.

Other applications of nanowires include using them as nano probes. This is something we have done as we develop GaN probes for SPM as described in section 4.3.

### 2.2.1. Oxidation

The gate of a MOSFET type device (described in section 2.1.4) is conceptually a capacitor. Since we want reasonable operating voltages for our transistor, when we make the area of a capacitor smaller we need materials with a higher dielectric constant to maintain a high enough amount of charge. Traditionally $SiO_2$ has been used but with the decreasing sizes of transistors we need to replace the $SiO_2$ with materials with even higher dielectric constant.

Two materials with higher dielectric constants that are frequently used are $Al_2O_3$ and $HfO_2$. The interface between InAs and $Al_2O_3$ is studied in **paper IV** where we evaluate a new approach to surface passivation by introducing an intermediate step of controlled thermal oxidation before ALD. ALD is described in section 2.2.3. We find that the amount of detrimental defects are reduced even though the thermal oxide is not yet stable to further oxidation during ambient conditions.

The interface between InAs and $HfO_2$ is studied in detail in **paper V** where we achieve time resolved measurements of the deposition of the very first atomic layers during ALD.

Even more studies of oxides are performed in **paper III** where we examine the oxide reduction upon H-plasma cleaning of GaSb substrates and nanowires.

### 2.2.2. Growth

To achieve the goal of materials with enhanced electronic properties we need to grow crystal structures of high quality with as few defects as possible. All nanowires used in the work included in this thesis were grown by our colleagues at the division of Solid State Physics at Lund University and, in the case of aerotaxy nanowires, by the company Sol Voltaics®.

There are several different growth techniques that yield crystal structures and especially nanowires[13]. I do not aim for a complete overview on the subject of growth since no growth was performed by me, but I rather aim to present a context to the growth of the different nanowires used in the work of this thesis.

The nanowires grown for this thesis have been grown in a bottom-up approach where atoms attach to each other building up the crystal nanostructure in a layer-by-layer fashion. In a crystal structure the atoms are arranged in an ordered structure as opposed to an amorphous material that lacks long range order. We often talk about epitaxy which is the ordered (-taxy) growth of one crystalline material on top (epi-) of another. Either the growth substrate is the same as the growing crystal (homoepitaxy) or there are two different materials (heteroepitaxy).

There are two main methods to control the growth dimensions of nanowires; growth through holes in a mask or using seed particle assisted growth. In the first method, growth through a mask, an insulating layer is covering the growth substrate and the growth is only conducted in openings in the mask. The dimensions of the grown nanowires are dependent on the dimension of the mask opening. This technique was used for the growth of the GaN nanowires used as SPM probes. In the second method, seed particle assisted growth (Figure 2.5), often a foreign metal (but sometimes the same material as the growth material[40]) is used as catalyst through which the supplied material is diffusing to finally build on the crystal. By far the most common metal catalyst particle material is Au but also other metals such as Ag can be used[41,42]. The dimension of the particle determines the dimension of the resulting nanowires. This technique was used for the growth of the aerotaxy GaAs nanowires presented in chapter 4.2.1 and the Au particles were examined *in-situ* as presented in chapter 4.2.2.

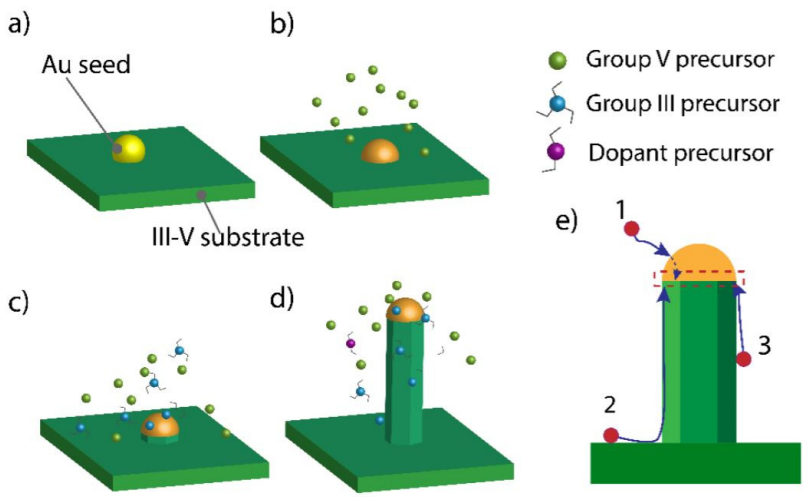


**FIGURE 2.5**
Schematic illustration of epitaxial particle assisted nanowire growth. In (a) a gold seed particle is deposited onto a growth substrate. (b) the sample is heated, the gold particle alloys with the substrate and the group V precursor is introduced. (c) The group III precursor is introduced and nanowire growth is commencing. (d) dopants are introduced. (e) the metal organic precursors can follow different diffusion paths to the nucleation site under the gold particle. They can (1) diffuse through the gold particle, (2) diffuse from the growth substrate, or (3) diffuse along the nanowire. (adapted from ref [43] with a bunch of fat stacks of credit attached)

*Epitaxy growth*

The fundamental idea of epitaxial growth is that atoms from a supply should be transitioned into a solid crystal phase. Historically the supply was most often in the form of a liquid and in that case it is known as Liquid Phase Epitaxy or, the more versatile technique, Solution Phase Epitaxy. In Molecular Beam Epitaxy (MBE) a beam of the elemental growth material is directed at the growth substrate[44].

The GaN nanowires used as probes in this thesis are grown by Metal Organic Vapour Phase Epitaxy (MOVPE) so this is the first technique I will focus on. MOVPE is also nowadays the most widely used technique for growing optoelectronic devices[45]. MOVPE is a subgroup of the more general technique Vapour Phase Epitaxy (VPE) where other molecules or elements than metal organic ones can be used for growth. This is in turn a subgroup of Chemical Vapour Deposition (CVD) where the growth is not necessarily epitaxial.

In MOVPE the supply is made up by a vapour of precursors (eg. trimethylgallium and ammonium ($NH_3$)). At a sufficiently high temperature and gas pressure the molecules crack and the C and H parts leave the III and V atoms to adhere to the growth surface. The adherence is energetically favourable as the chemical potential of the gas is higher than that of the substrate. Consequently, the molecules in the gas seek to lower their chemical potential by adhering to the surface and hence growth is commenced.

The GaN nanowires to be used as SPM probes were grown by selective-area epitaxy with metal-organic CVD which had to be conducted in a 3-step process. Their structure is described further in section 4.3.1. First, the nanowire core was grown keeping the ammonium level low, this results in a core with low conductance. Secondly an under-layer is grown, covering the core, using higher levels of ammonium resulting in high quality conducting GaN with a sharp tip. At last a second under-layer is grown, enhancing the amount of high quality material radially.

*Aerotaxy growth*

Aerotaxy is an aerosol-based growth method with a seed particle. The word itself, aerotaxy, is a combination of *aerosol* and *epitaxy* which describes the phenomenon well. The aerotaxy technique is revolutionary in the sense that it is conducted without the expensive and limiting crystal substrates that is the trademark of epitaxial growth. Instead the nanowires, or more generally nanostructures[46,47], are grown from an aerosol of seed particles dispersed in a continuous gas flow[14]. The process is depicted in Figure 2.6. First the Au seed particles are generated, size selected and sintered. Then the growth material is introduced and the nanowires are grown by diffusion through the aerosol particles.

During this step there is a possibility to incorporate dopants by supplying yet another precursor. Last the nanowire are randomly deposited and collected on a substrate of any type. The growth rate is a remarkable 20 to 1000 times higher than for epitaxial growth which is important from an economic point of view and makes the technique highly relevant for mass production of nanowires. Using aerotaxy growth it is also possible to achieve higher doping levels since the out-diffusion of the dopants to a substrate is not viable.

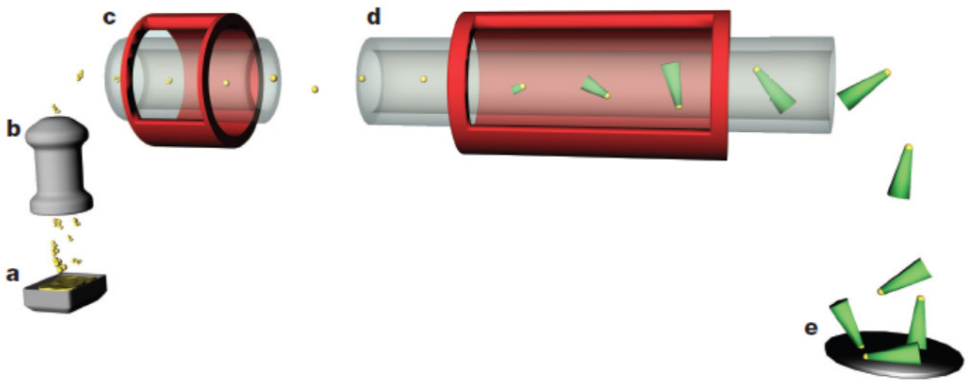


**FIGURE 2.6**
Schematic illustration of the aerotaxy growth process. Au particles are (a) generated, (b) size selected and (c) sintered in order to constitute as seed particles for the aerotaxy growth. In (d) the precursor gases are introduced and during advantageous pressure and tepmerature the nanowires start to grow. (e) After growth the nanowires are deposited on a surface. (adapted from [14])

Aerotaxy nanowires have been grown with different materials (eg. GaAs, GaAsP)[48,49] and doping (eg. Sn, Zn)[50,51] and they have been grown with *pn*-junctions[52] and their recombination dynamics has been studied[53] but still not much is known about their surfaces which is addressed in **paper I**.

### *Atomic Layer Deposition*

Atomic Layer Deposition (ALD) is a sub-group of CVD where molecules in gas phase react with a surface resulting in the deposition of ultra-thin, self-limiting layers of material. ALD is now a standard technique used in device fabrication where its main purpose is to deposit thin films of high-*k* oxides.

The chemicals used in the process are called *precursors* and are introduced alternately in cycles. A full cycle of deposited material consists of two half-cycles where during the first half-cycle one of the precursors (e.g. tetrakis-dimethylamino hafnium (TDMA-Hf)) flows through the reaction cell. After reaction of the first precursor the cell is pumped to vacuum before the second half-cycle (of e.g. $H_2O$) is conducted. In **paper IV** and **paper V** we study the effect of ALD on InAs.

### 2.2.3. Hardness

The mechanical integrity of a material is highly relevant for its capacity to function well as an SPM probe. Mechanical properties, such as hardness or stiffness become important. Hardness is a measure of how well a material can withstand localized plastic deformation (which is really a surface feature). Therefore I will here give a brief summary on the subject of hardness.

There are several common tests for measuring hardness. It is a measure of how well a material resists plastic deformation. A higher hardness means higher resistance to being permanently deformed. There exists a variety of tests such as for example Rockwell, Brinell, Barcol, Vickers, Knoop, Shore and Mohs hardness tests where Rockwell is the most applied one.

Common to most of these tests (e.g. Rockwell etc.), is that an indentation is made with a sphere or pyramid and the applied force used to make the indentation is measured to evaluate the hardness of the material.

Relevant for an SPM probe is however how resistant the probe is against scratching and abrasion during its sweeping motions across a sample surface. A test that measures exactly this is Mohs hardness test. In Mohs hardness test a material is scratched with a reference material of known hardness[54]. There are 10 reference materials and they are shown in Table 2.1. If a material is scratched by quartz but not by orthoclase its hardness is between 6 and 7.

**Tabel 2.1. Mohs hardness Scale**
The reference minerals and its corresponding Mohs hardness given by definition.

| Reference mineral | Mohs Hardness |
|---|---|
| Talc | 1 |
| Gypsum | 2 |
| Calcite | 3 |
| Flourite | 4 |
| Apatite | 5 |
| Orthoclase | 6 |
| Quartz | 7 |
| Topaz | 8 |
| Corundum | 9 |
| Diamond | 10 |

When using Mohs hardness one must be aware that the values given to the reference minerals do not scale linearly and hence an increase from 4 to 5 is not comparable to an increase from 7 to 8 making comparisons between material values not trivial. The hardness of GaN is 7 on Mohs hardness test. 7 is, generally speaking, a high number compared to other tip materials such as Pt (3.5), Au (2.5), W (7.5) and Si (6.5)[55].

# 3. Experimental methods

In chapter 3 I present a brief description of the characterization methods and instruments used in the work of this thesis. Scanning Tunneling Microscopy was used in **paper II**, Atomic Force Microscopy was used in **paper I** and **paper II**, X-ray Photoelectron Spectroscopy was used mainly in **paper I, III, IV** and **V** Small Ange X-ray Scattering (SAXS) was used in **paper VI**.

In most of the work included in this thesis we perform studies of surfaces and interfaces. We aim to map the surface various length scales. First on a longer range, to get an idea of the overall morphology over several of micrometers of both nanowire surfaces and flat surfaces, secondly on a more local, short range to learn about surface steps and even atomic structure on an Ångström scale. Therefore, we need surface sensitive methods covering all the way from micrometer scale down to sub nanometer scale. For this AFM and STM are helpful. With AFM we can quickly get a good overview of the morphology of a sample from micrometer to nanometer range. For even smaller range and for additional knowledge of the electronic properties of the sample we use STM. Using XPS we get chemical surface composition and knowledge about the different elemental species and their chemical surroundings. Lastly, with SAXS we gain knowledge about the shape and size of the nanostructures. These four methods also have different probing widths, from segments of nanowire surfaces probed with STM to full individual nanowires with AFM to large ensembles of nanowires or nanostructures with XPS and SAXS.

## 3.1. Scanning Tunneling Microscopy

In this section I give an introduction to STM including a hands-on description of the instrument as well as theory behind the physical phenomena involved. I

present the common ways of preparing an STM probe. I also introduce STS and discuss the differences occurring while using a metallic tip contra a semiconducting tip and scanning or performing spectroscopy on metallic or semiconducting surfaces.

1981 marked the beginning of a new era for surface science as Binnig and Rohrer invented the STM. Their invention allowed researchers to finally image surfaces on an atomic scale. Binnig and Rohrer were awarded the Nobel Prize in physics in 1986 for their development of the technique.

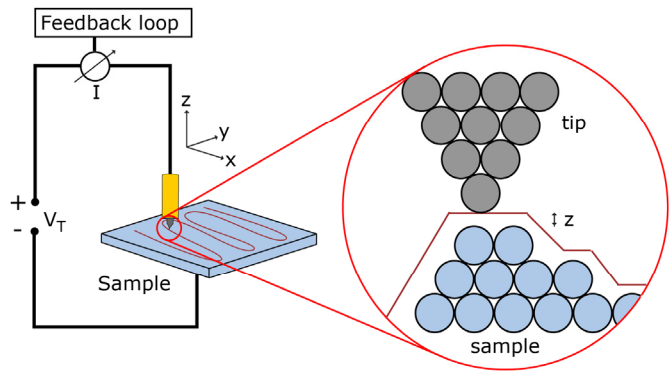


**FIGURE 3.1**
Schematic illustration of an STM setup. A sharp, conducting tip is brought close to, and swept over, a conducting sample surface. A bias, $V_T$, is applied over the system and the resulting tunneling current is recorded. The tip-sample separation is marked by z.

STM utilizes quantum mechanical tunneling of electrons between a sharp, conducting, needle like tip and a sample surface. Using STM it is possible to map the density of electronic states of a sample surface[56]. In Figure 3.1 the schematics of an STM is pictured. The tip is brought into close proximity, usually less than 1 nm, of the sample surface. A bias is applied over the tip and the sample inducing a tunneling current, usually with a magnitude in the order of pA to nA, to run through the system. The tip is coupled to a feedback loop and piezo electrical crystals change the tip-sample separation to maintain a pre-defined set-point current, *I*. The tip is raster scanned and in each point of the raster the z-piezo signal is measured and a computer software draws the corresponding height map of the surface. The imaging contrast is described in more detail later but the measurements are strongly localized with a very high spatial resolution that is dependent on the tip apex radius of curvature and a sub-Ångström vertical resolution as explained by equation 3.1.

### 3.1.1. Theory

The foundation of STM measurements is quantum mechanical tunneling. In classical physics a particle is not allowed to cross a barrier. We can think of it much as we think of a ball bouncing off a wall. In quantum mechanics, which we need to describe phenomena on a microscopic scale, particles have both particle-like and wave-like properties. Our ball, the electron, can also be described as a wave and will have a small probability to pass through the wall. The thinner the wall the higher is the probability of a transfer. The electrons are said to be tunneling. This is taken advantage of in STM where a tip is brought into close proximity to a sample surface, separated only by a thin vacuum barrier of down to sub-nanometer length, $z$. Though not in classical contact with each other, electrons in both the tip and the sample, described as wave functions and following the Schrödinger equation, are allowed to tunnel through the vacuum barrier creating a tunneling current between the tip and the sample. The high vertical resolution of STM is derived from that the tunneling current $I_T$ has been shown to decrease exponentially with the tip-sample separation, $z$, as:

$$I_T \propto e^{-2z\kappa}, \qquad \text{(Eq. 3.1)}$$

which is a one dimensional solution to the Schrödinger equation and with κ, the inverse electron decay rate:

$$\kappa = \hbar^{-1}(2m\Phi(V_T))^{\frac{1}{2}}, \qquad \text{(Eq. 3.2)}$$

where $m$ is the electron mass, $\hbar$ is Planck's constant and $\Phi(V_T)$ the effective local work function, depending on the bias, $V_T$, applied to the sample.

We can dive even further into the theory behind STM measurements by looking at the electron transfer between the sample and the probe[57,58]. Fermi's golden rule gives the probability of electron transfer between an initial state $E_i$ and a final state $E_f$ across a vacuum barrier of width $z$ and is given by:

$$T = \frac{2\pi}{\hbar}\left|M_{i,f}\right|^2 \delta(E_i - E_f), \qquad \text{(Eq. 3.3)}$$

where the delta function ensures that we only consider transfer between states of the same energy, disregarding the creation and effect of, for example, phonons and plasmons or other types of inelastic interactions. The matrix element $M_{i,f}$ will be introduced below.

Now that we have the probability of transfer we can also give an expression of the tunneling current, $I_T$. To do so we can use first order perturbation theory and express it as:

$$I_T = \left(\frac{2\pi e}{\hbar}\right)\sum_{i,f} f(E_i)\left[1 - f\left(E_f + eV_T\right)\right]\left|M_{i,f}\right|^2 \delta\left(E_i - E_f\right), \qquad \text{(Eq. 3.4)}$$

Note how we by using perturbation theory now include the dependency on the energies of the tip and the sample via the Fermi Dirac distribution function, $f(E)$ and also the applied bias, $V_T$.

Tunneling has a chance to occur wherever the wave functions in the tip and the sample overlap which they will do if the distance, $z$, between them is sufficiently small (in the order of sub nanometer length). To find this overlap we then solve the Schrödinger equation for electrons in both the tip and the sample separately. The overlap of these solutions can then be expressed by, the above mentioned tunneling matrix element, $M_{i,f}$ as an integral over an arbitrary 2D surface located anywhere between the tip and the sample:

$$M_{i,f} = -\frac{\hbar}{2m}\int\left(\psi_i \nabla\psi_f - \psi_f \nabla\psi_i{}^*\right)dS, \qquad \text{(Eq. 3.5)}$$

where only the overlapping matrix elements are non-zero. But the initial and final states of the wave functions ($\psi_i$ and $\psi_f$), needed to calculate $M_{i,f}$, are generally not known and not at all trivial, leading us to make a few assumptions about the system in order to continue.

**Assumptions of tip properties**

- The tip has a low temperature.
- The main contribution to the tunneling current arises from an s-type orbital.
- The tip has a spherical apex.
- The tip is spatially and energetically isotropic.

With these assumptions Tersoff and Hamann has shown that the tunneling current is proportional to the integrated density of states (IDOS) at the position $r_0$ of the tip as[59]:

$$I_T \propto \rho_t \int_{E_F=0}^{eV_T} \rho_{s,loc}(\overrightarrow{r_0},\, E_F + \varepsilon)d\varepsilon, \qquad \text{(Eq. 3.6)}$$

where $\rho_t$ and $\rho_{s,loc}(\overrightarrow{r_0},\, E_F + \varepsilon)$ are the local density of state (LDOS) of the tip apex atom and the LDOS of the surface at position $r$ and energy $E$ respectively.

Note that the limits of the integral are the Fermi level, $E_F$, and the applied bias, $V_T$, which tells us that the current is proportional to the LDOS around the Fermi level.

So, Eq. 3.6 explains what an STM image of a flat sample surface is, i.e. a map of the LDOS of the system. The system here includes both the tip and the sample which is why STM images are greatly affected by tip changes. The deconvolution of the signal originating from the sample can be challenging. Areas with a lot of available states to tunnel to or from (depending on the sign of the applied bias) will generate a higher current (and appear bright in the image if conventional color coding is used). As a consequence, a semiconductor with a smaller bandgap will at a given tunnel bias appear brighter than a material with a larger bandgap at the same surface height. For larger structures however the dominating effect will come from height changes (remember the z-dependency from Eq. 3.1) and the image can be interpreted as a height map.

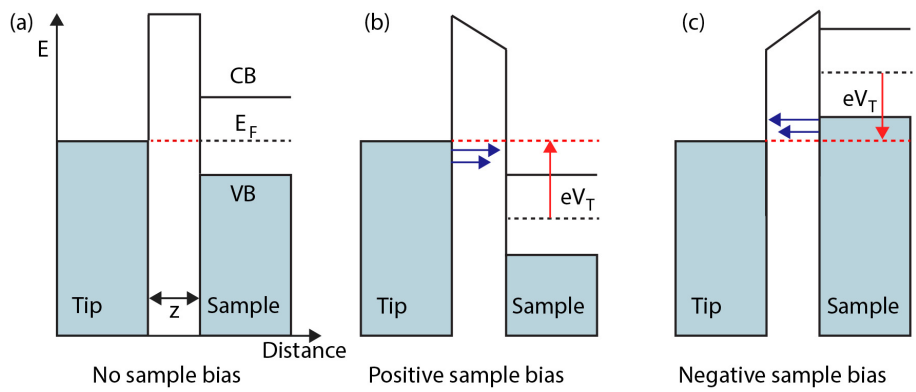


**FIGURE 3.2**
Energy diagram for a metallic tip and a semiconducting sample at (a) no applied bias, (b) positive sample bias and (c) negative sample bias. The conduction band (CB), valence band (VB) and the tip-sample separation (z) are marked in the figure. The Fermi level, $E_F$, is marked by a dotted black line. In the cases where a bias is applied over the system the difference in energy between the Fermi level of the metallic tip and the Fermi level of the semiconductor is marked by $eV_T$ and indicated by a dotted red line and a red arrow.

In Figure 3.2 energy diagrams depicting a metallic tip and a semiconducting sample are shown. The tip and the sample are separated only by a small distance, $z$, and the energy diagrams shows three different cases, (a) no bias applied to the system, (b) a positive bias applied to the sample and (c) a negative bias applied to the sample. In the first case where no bias is applied to the system the Fermi levels of the tip and the sample are aligned. No tunneling occurs in this case. In the second case, where a positive bias is applied to the sample, electrons will tunnel from filled states below the Fermi level of the metallic tip into the conduction band of the semiconducting sample where empty states are located. In this case we are imaging empty states in the sample. In the third case, where a negative bias is

applied to the sample, electrons will instead tunnel from filled states in the sample to empty states above the Fermi level of the metallic tip. In this case we are imaging filled states of the sample.

For a III-V semiconducting sample the electron orbitals corresponding to filled and empty states are reported to be localized around one element each[60]. The empty states are found around the group III atoms and the filled states are found around the dangling bonds of the group V atoms, giving an elemental specific image contrast. This means that when we are imaging a metallic surface with a semiconducting III-V GaN tip (careful now, as we switch place on the tip and the sample) and apply a negative bias to the sample, the electrons are tunneling from the sample into empty states located around the dangling bonds of the Ga atoms in the tip. Vice versa, with a positive sample bias we mainly use electrons from the filled states around the N atoms to tunnel into the empty states above the Fermi level in the sample. The latter case has generally given the most stable imaging conditions.

### 3.1.2. Practice

The STM, though a highly sophisticated tool, consists of only a few parts. Even so, it is not a simple instrument to construct due to the small distances, currents and level of vibrational control involved in the measurements.

**Necessary parts of an STM**

- A sharp and conducting tip.
- Vibrational control.
- Position control.
- Computer control software with feedback loop.
- A pre-amplifier.

There are different types of vibrational control, for example suspension with magnets or springs and damping, pneumatics or stacked plates. The position needs to be controlled for both the tip and the sample. Usually both a coarse position control in the form of a mechanical positioner and fine position control provided by piezo electric devices are used. A computer with software and a feedback loop controlling and monitoring the tip-sample interaction is needed. Historically the feedback loop was external and not part of the computer software.

The most important parameters that the STM operator has to play with to obtain a nice image (a typical STM image is shown in Figure 3.3) are the bias, $V_T$, the

current set point, $I_{set}$, and the loop gain. The bias applied when using a metal tip and scanning a semiconducting sample is usually around $\pm 1 - 3V$. For a semiconducting tip on a semiconducting sample one has to be careful though and make an estimation of the size of the combined band gaps of the sample and the tip. The current set point determines not only the desired value for the feedback loop but also the distance between the tip and the sample as explained by Eq. 3.1. A typical value for the set point is between 30 pA and 300 pA for a semiconducting sample. It is the difference between the set-point and the measured value that is used to control the height position of the tip. The loop gains, consisting of the derivative, proportional and integral gain determine how the height value is updated and hence how quick the feedback loop will react to height changes in the sample structure. Normal values ranges between 0.1% and 5% depending on the expected height variations of the sample surface. A higher loop gain will give quicker reactions but will also induce unwanted vibrations. A high loop gains is a great tool when expecting to encounter abrupt height changes like when searching for nanowires on a substrates.

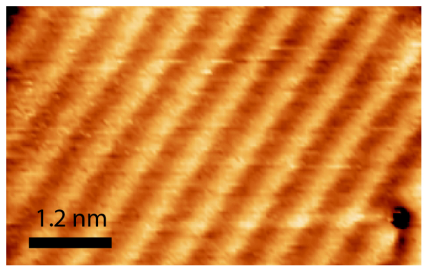


**FIGURE 3.3**
STM on a GaAs aerotaxy nanowire. The surface is an unreconstructed (110) surface aqcuired at a current set point of $I_{SET}$=30 pA and a gap voltage of $V_T$=-3.3 V.

### 3.1.3. Scanning Tunneling Spectroscopy

Scanning Tunneling Spectroscopy has been a pivotal tool in the work with the GaN nanowire STM probes. STS has come to work as a way of confirming the presence of the GaN nanowire on the tip. A detailed understanding of the GaN probe–sample interaction is yet to be explored but also here I expect STS to be of great importance. Here I aim to give an introduction to the technique and to briefly discuss interpretation of spectroscopy data.

Spectroscopy can be performed by decoupling the feedback loop of the system and keeping a fixed position over the sample surface. The voltage can then be swept at a single point and the tunneling current recorded as a function of the applied tip-sample bias. In other words, this means that we can record the current as a function of the applied voltage and obtain a map of the IDOS around the Fermi

level. A voltage applied to the sample sweeping from negative to positive will therefore give us the filled states below the Fermi level for negative voltages and the empty states above the Fermi level for positive voltages.

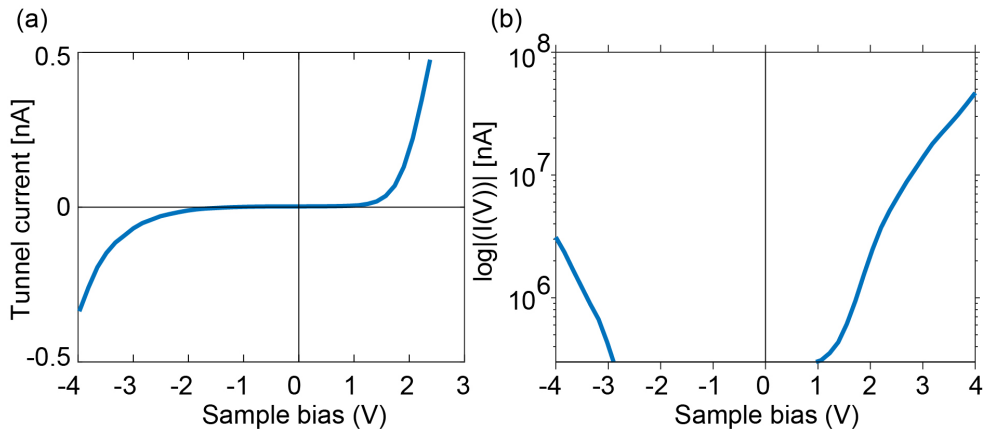


**FIGURE 3.4**
STS with a GaN probe on Au(111). (a)The spectrum is an average of 95 individual spectra. It shows the measured tunnel current plotted against the voltage applied to the sample. In (b) is a log plot of the absolute value of the spectrum in (a).

During the work with the GaN nanowire STM/S probes a lot of STS has been performed on various substrates. STS with a GaN nanowire probe on Au(111) is shown in Figure 3.4. The spectrum in (a) shows the tunnel current plotted versus the sample bias. For visibility of the band onsets the data is often displayed as in (b) which shows the logarithm of the absolute value of the spectrum in (a).

*Tip induced band bending*

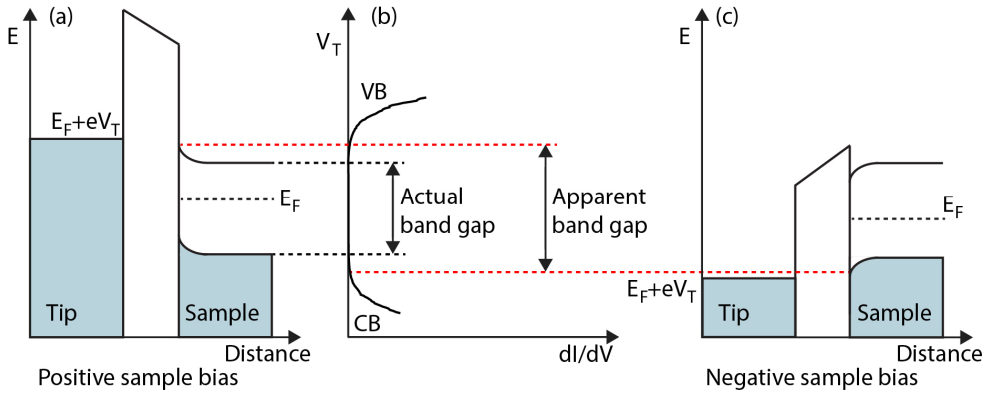


**FIGURE 3.5**
Energy diagram for a metallic tip and a semiconducting sample illustrating the effect of tip induced band bending on the measured band gap. In (a) the bands in the sample are bent slightly upward as a positive bias is applied. In (c) we see the reverse situation with a negativ sample bias. In (b) the actual band gap and the apparent (measured) band gap are shown. The Fermi level ($E_F$), the valence band (VB) and the conduction band (CB) are all marked in the figure.

Semiconductors are dielectric by nature and an applied electric field will cause the semiconductor to polarize. When a metallic tip with an applied bias is brought close to a semiconductor the polarization will cause the bands in the semiconductor to bend towards the Fermi level of the tip. This effect is called tip-induced band bending and needs to be considered when interpreting STS data. The apparent, or measured, band gap will appear bigger due to the band bending. This is explained in Figure 3.5 where the apparent band gap ranges all the way from the top of the upwards bent conduction band (as in Figure 3.5 (a) when a positive bias is applied) to the bottom of the downwards bent valence band (as in Figure 3.5 (c) when a negative bias is applied). The band bending depends on several physical interactions between the tip and the sample, such as the tip-sample separation, their relative Fermi level and the applied bias. Properties that affect these are for example the shape of the tip, the tip work function, the carrier concentration in the sample and the electron affinity.

### 3.1.4. STM probes

STM is completely dependent on the probe and the probe properties. Traditionally probes for STM most often consist of tungsten (W) or platinum/iridium (Pt/Ir) though Au is also used. There are several different methods for producing STM probes. In section 4.3 I describe a novel production method manipulating a nanowire onto an STM probe. Here I want to introduce the most common method

of probe production which is by electrochemical etching of a metal wire. Other ways include cutting or mechanical shearing of a wire. Usually probe preparation also includes Argon sputtering or annealing of the tip to reduce etching-induced oxides, residues and surface contaminations.

### *Etching of STM probes*

Most of the W probes for STM used in this work were prepared by electro chemical etching of 0.38 mm diameter polycrystalline W wire. A commercially available setup (Omicron) for DC electrochemical tip etching was used and the process is depicted in Figure 3.6.

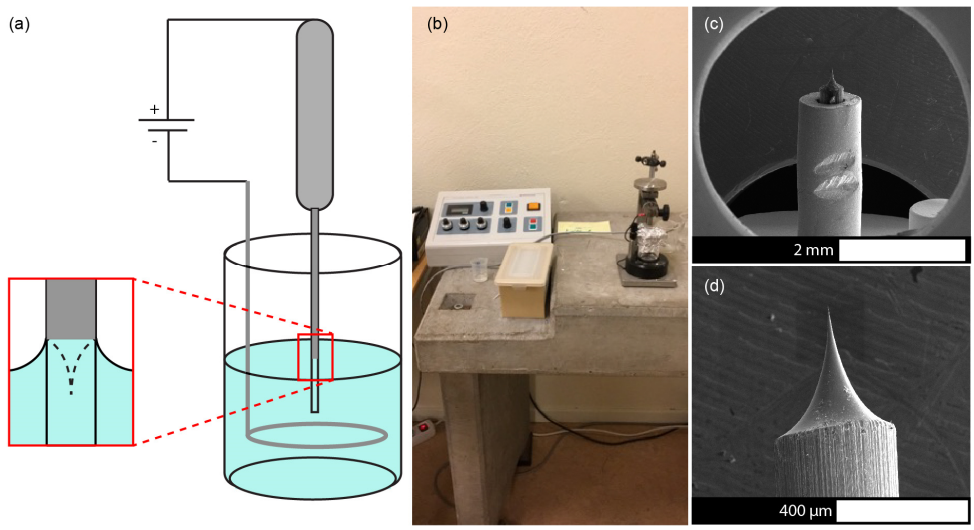


**FIGURE 3.6**
(a) A sketch of the tip etching set-up. (b) The tip etching station. (c)-(d) SEM images of an etched tungsten wire clamped in place in its holder.

The W wire acts as the anode, a ring of stainless steel acts as the cathode and the electrolyte is sodium hydroxide (NaOH). $H_2$ is produced at the cathode. A voltage is applied and electrons run from the W anode to the stainless steel cathode resulting in an ionization of the W atoms. The ionized surface atoms react with oxygen and the formation of $WO_2$ occurs as follows[61]:

At the anode:

$$W(s) + 8OH^- \rightarrow WO_4^{2-} + 4H_2O + 6e^- \qquad \text{(Eq. 3.7)}$$

At the cathode:

$$6H_2O + 6e^- \rightarrow 3H_2(g) + 6OH^- \qquad \text{(Eq. 3.8)}$$

Which in total gives[62]:

$$W(s) + 2OH^- + 2H_2O \rightarrow WO_4^{2-} + 3H_2(g) \qquad \text{(Eq. 3.9)}$$

The W wire, which is etched predominantly at the electrolyte/air interface, gets thinner and thinner and finally cuts off at the surface. The lower part falls down and the electric circuit is broken. The optimal etching settings depend on the concentration of the solution and how many tips have been etched in it (since the solution gets consumed by the etching). We routinely achieve good STM probes by using a 2 mol/liter concentration of NaOH, an etching voltage of 9 V and a threshold current of 1.5 mA.

*Post-processing*

There are a few post-processing procedures that are routinely performed in order to minimize etching residue and surface oxides on the tip. Immediately after etching, the tip is rinsed with distilled water and ethanol to reduce the amount of etchant residue. Sputtering with argon, for 30 minutes at a pressure of $2\text{x}10^{-5}$ mbar, is done in vacuum, with a base pressure of around $10^{-9}$ mbar, to get rid of the thick oxide of the tip. The acceleration voltage for the argon gun is set to 3 kV and the emission current is set to 20 mA. This is performed twice, first with the tip pointing towards the argon gun and then a second time pointing away from it.

## 3.2. Atomic Force Microscopy

The development of the Atomic Force Microscope (AFM) followed closely after the invention of the STM. In 1985 Binnig et al. combined the principles of the STM with the stylus profilometer and the result was a microscope that was no longer dependent on conductivity of the sample but rather contours the top layer of the sample surface[63]. The AFM quickly became a widely used tool in surface science and is now considered one of the standard instruments for surface characterization. The AFM is slightly more flexible than the STM since it can be used on non-conductive surfaces. High resolution is more challenging to obtain using an AFM compared to using an STM, but it is possible to achieve atomic resolution[64].

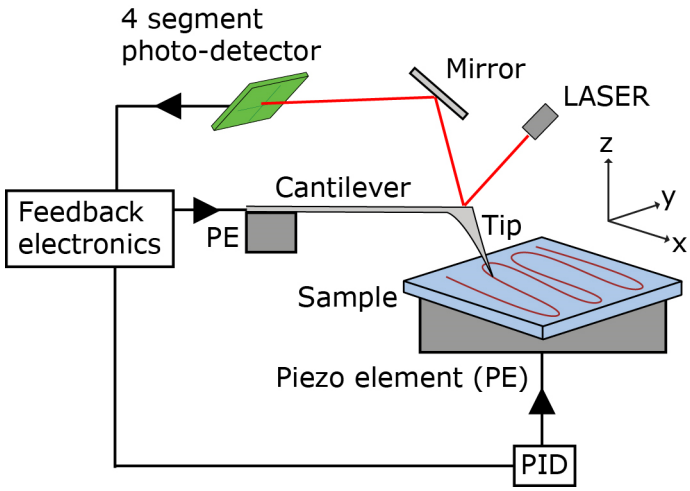


**FIGURE 3.7**
Sketch of the AFM set-up. A laser hits the back of the tip and is reflected onto a mirror and guided to a detector. PE denotes the Piezo electric elements used to control the tip and sample movement. PID is the proportional, integral and derivative gains used in the feedback loop.

In AFM a sharp needle attached to a cantilever is brought into close proximity to a sample surface[65]. The system is depicted in Figure 3.7. Piezoelectric devices are used for the approach and positioning of the tip. A laser tracks the tip deflection and is registered by a photo-detector. A feedback loop, with integral gain and proportional gain, reads the deflection and adjust the piezo z position of the cantilever over the surface. A map of for example the deflection or piezo z position after feedback is drawn and shown to the user.

### 3.2.1. Theory

AFM images are acquired by measuring the forces between the tip and the sample[65]. There are several forces involved and they can be divided into repulsive and attractive forces with a long or short range. The main attractive forces involved are Van der Waals forces, capillary forces (in air), electrostatic forces, covalent forces and the main repulsive force arises from the fact that the electrons of the atoms are fermions and due to the Pauli exclusion principle cannot inhabit the same space simultaneously. Another force is the electron-electron Coulomb interaction which originates from that two particles with the same charge repels each other. It is more long range than the Pauli exclusion principle and it can be either attractive or repulsive depending on the charges involved Generally the repulsive forces are short length with a quick decay with distance.

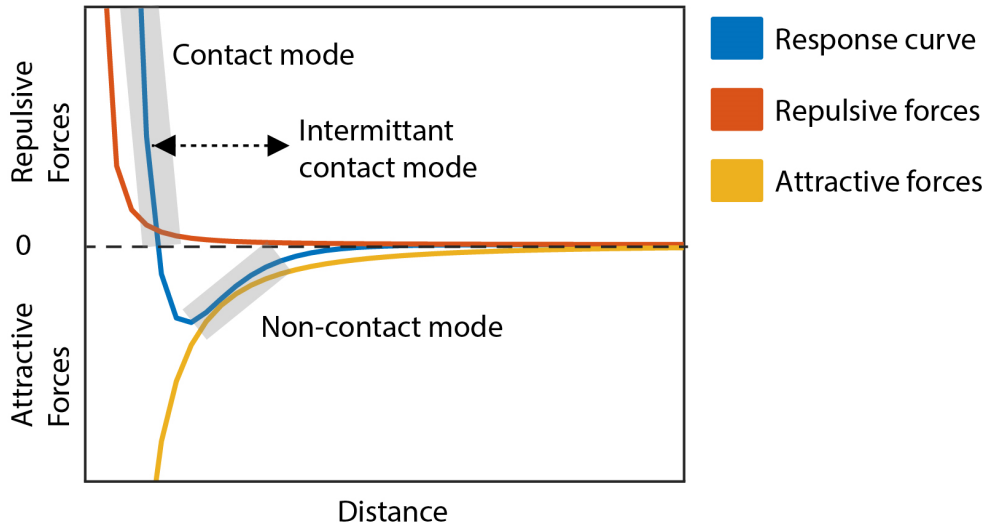


**FIGURE 3.8**
The forces involved in an AFM measurement. (red) The repulsive forces (originating from the Pauli exclusion pricniple), (yellow) the attractive forces (dominated by the Van der Waals interactions) and (blue) the resulting force response curve.

There are several standard working modes of AFM. They are divided into contact, non-contact and intermittent contact mode, ultimately describing the interaction between the scanning medium and the sample. The working regions of these modes are described in Figure 3.8 where we assume that the tip is brought from far away towards the sample surface (e.g. from right to left in the graph). First it starts seeing long range, attractive forces and eventually, when it gets close enough, it sees also repulsive forces. In contact mode the tip is brought into the repulsive region of the sample, hindered by Coulomb forces and Pauli exclusion principle. In this mode a force, usually in the order of nN, is applied onto the sample surface. In non-contact mode the tip is held completely out of the repulsive region and made to work only in the attractive region effectively not altering the sample surface at all. In intermittent contact mode the cantilever is driven to resonate at its Eigenfrequency. The tip is brought into close proximity of the surface and is made to tap in and out of the repulsive region. Intermittent contact mode is less damaging than contact mode where the tip might scratch a soft surface despite the small forces involved.

### 3.2.2. Practice

The AFM, like the STM, consists of only a few parts.

**Necessary parts of an AFM**

- A sharp tip attached to a cantilever.
- Position control.
- Computer software with feedback loop.
- Detection of cantilever movements.
- Vibrational control.

An AFM tip consists of a cantilever chip and a cantilever with a tip at its end. The most common probe material is Si coated with metals for enhanced reflectivity and/or conduction. Various probes for optimized scanning on samples of different types exist. The requirements on a probe used to scan biological tissue are different from the ones on a probe used to scan hard materials such as metals or semiconductors[66,67]. In this work we have focused on developing a probe tailor made for incorporating light and for detailed knowledge of the probe morphology to be able to de-convolve the resulting images and get a better understanding of the true sample structure.

The tip and sample position and movements need to be carefully controlled. This is achieved by using piezo electric materials, most often in the form of a rod structure.

Commercial AFM systems come with their own computer software for imaging and user control. During this work we have mainly used a JPK nanowizard AFM operated in intermittent contact mode. For image and data treatment we have used WSxM or Gwyddion. For data treatment we routinely use plane correction and levelling of the images to get rid of any effect arising from the tip and the sample not being perpendicular to each other during imaging.

Several detection systems exist in commercially available AFMs, the most common ones being laser detection and tuning fork detection. In laser detection mode a laser is directed onto the backside of the cantilever. The laser is reflected from the backside of the cantilever onto a mirror which directs the laser onto a four quadrant photodetector. This allows for detection of changes in the deflection, vibration amplitude and also phase between the drive signal and the cantilever.

To achieve high resolution scanning the AFM also needs vibrational control. Often the AFM is placed on a pneumatic table for this purpose.

AFM phase imaging is a valuable tool for imaging surfaces and facets of nanowires. The phase measures the difference between the drive signal and the cantilever oscillation. In phase imaging the energy dissipation in the interaction between the tip and the sample is measured[68]. Energy dissipation can have several different reasons and hence several different phenomena can give contrast to a phase image. A tip sweeping a surface containing patches of varying materials can give contrast if the different materials have different adherence or "stickiness". Another source of contrast is the contact area between the tip and the sample. The contact area will vary depending on the angle between the tip and the sample surface; hence slopes, also very small slope variations, will be clearly visible in phase imaging. This is of great value when examining the topography of the facets of nanowires.

## 3.3. X-ray Photoelectron Spectroscopy

Heinrich Hertz, who earlier proved the existence of electromagnetic waves, discovered in 1887 that a material can emit electrons if irradiated with light[69]. This was the ground for the discovery of the photoelectric effect described by Albert Einstein in 1905[70] which granted him the Nobel Prize in physics in 1921. Taking it one step further by using monochromatic waves of light and detecting the kinetic energy of the excited electrons Kai Siegbahn finally developed the technique that we now know as X-ray photoelectron spectroscopy (XPS). He was awarded the Nobel Prize for it in 1981.

The technique of shining light onto a sample and detecting the excited electrons is not confined to work for only X-rays. A wide range of energies of light can be used that spans UV light, soft X-rays and hard X-rays. In this section I will focus on the technique using soft X-rays (which is roughly the range between 100 and 3000 eV). Photo excited electrons in a material can both be directly emitted, inelastic scattered (and still be emitted) or result in further electron emission. From now on I will consider the case of directly photo emitted electrons where the kinetic energy of the exciting photon is conserved.

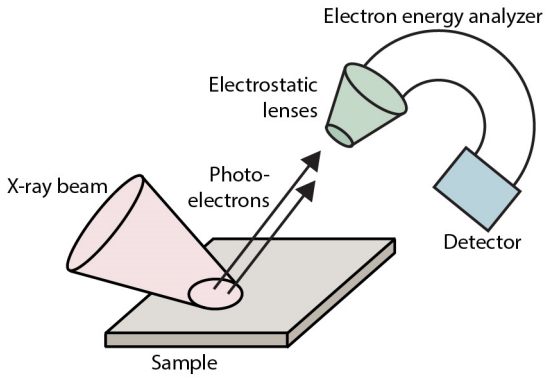


**FIGURE 3.9**
A schematic representation of an XPS set-up. A beam of X-rays is directed onto a sample. Electrons escaping the sample are collected by an electron energy analyser and counted by a detector.

**Basic parts for XPS**

- X-ray source.
- Electron energy analyzer.
- Detector.

A sketch of an XPS set up is shown in Figure 3.9. An X-ray beam is directed upon a sample and electrons escaping the sample are collected by an electron energy analyzer where electrons with selected energy are further directed onto a detector. The selection of electrons with a specified energy is often done as follows. In an electron energy analyser the electrons travel through an electric field which will bend the electron trajectory. How much the electron trajectory is bent depends on the electron energy. Electrons with too high or too low energy will hit the walls of the analyzer and never reach the detector. This allows us to detect electrons with a specified energy. The detector is usually a multi-channel-plate and CCD with the purpose of imaging (and then counting) the number of impinging electrons in a certain angular range, which represents a certain energy window. By sweeping the voltages of the electron energy analyzer it is possible to measure the intensity of the electron flux as a function of the kinetic energy of the electrons. Hence we can localise peaks corresponding to specific atomic core-levels as described in a bit.

XPS experiments are traditionally performed with lab sources as the photon source. The most commonly used X-ray generating lab source is probably an X-ray tube with an Al anode emitting X-rays with a photon energy of 1486.7 eV.

However during the work with this thesis only X-rays generated in synchrotron facilities have been used, which will be discussed below.

XPS is elemental and chemical specific and offers the opportunity to study not only the elements in a sample surface, but also their chemical surrounding[71]. Additionally, XPS can be used to quantify the relative amounts of different chemical species and elements. It is a highly surface sensitive technique due to the short inelastic mean free path of the photoelectrons which can also be used to quantify the material composition perpendicular to the surface down to ~5nm.

### 3.3.1. Theory

In Figure 3.10 the energy diagram of the photoelectron process is shown. X-rays with energy $h\nu$ are impinging upon a sample and transfer energy to an electron that gets excited into vacuum if the energy of the impinging photon is high enough. Depending on the supplied energy the electrons can be excited only from the valence band (green filled circle in Figure 3.10) or additionally from the core levels (red filled circle in Figure 3.10). Lower energies can excite electrons from the valence band since they are loosely bound. Higher energies can excite also core level electrons originating from electronics states more closely bound to the atom core. If the supplied energy is high enough to let the electrons overcome the work function threshold (or the vacuum level $E_{VAC}$) and escape the sample with a kinetic energy $E_k$, they can be detected and analyzed.

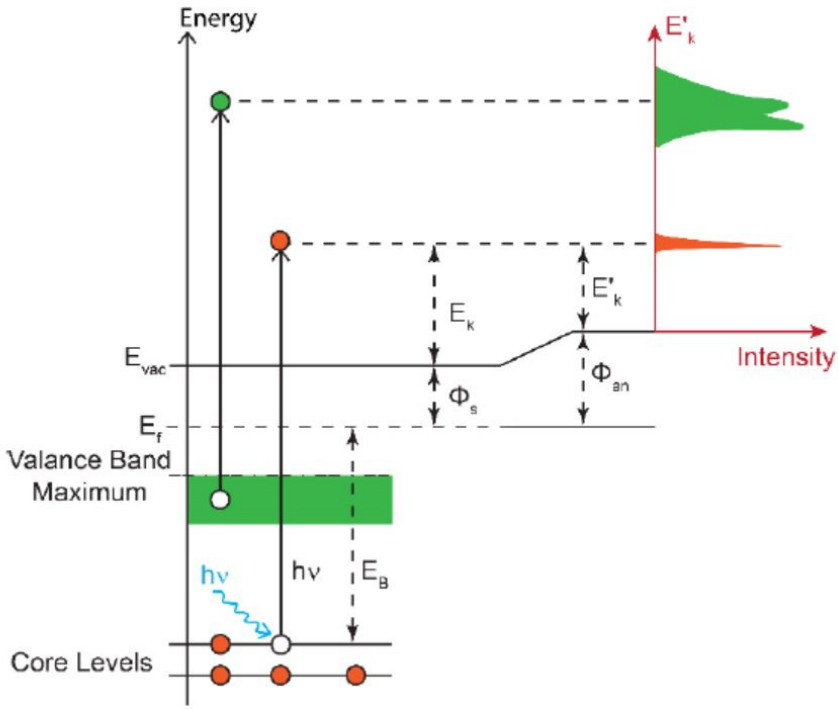


**FIGURE 3.10**
Energy diagram of the involved energies in the XPS process. . On the right the energy levels in the material is seen, while on the right the resulting spectrum measured in XPS is displayed. An electron from a core level (red circle) gets excited by the added energy of the impinging X-rays (marked hν). Electrons in the valence band (green circle) can also get excited. The Fermi level ($E_F$), the vacuum level ($E_{VAC}$), the kinteci energy of the electron ($E_k$), the binding energy ($E_B$) and the work function of the sample and the analyzer ($\Phi_S$ and $\Phi_{an}$ respectively) are all marked in the figure. The effective workfunction is a combination of these two. (adapted from [72]).

We measure the kinetic energy of the electron $E_k$, we know the energy of the impinging photons, $h\nu$, and hence we can determine which binding energy the electron had in its initial state. The binding energy, $E_B$, of an electron is given by:

$$E_B = h\nu - E_k - \Phi \qquad \text{(Eq. 3.10)}$$

where Φ is the work function which is defined as the amount of energy it takes to excite an electron from the Fermi level, $E_F$, to the vacuum level $E_V$ – a value that is not known. The work function of the analyzer is generally not known but it is necessary in order to calculate the measured absolute binding energy of the electrons. Therefore, a thorough calibration is needed. In the work within this thesis the absolute binding energy position has never been a main concern. The interest has rather been relative binding energies, shifts, between components of the same core level. Anyhow calibration of the energy position has been done. For a metal, the Fermi Level can be used as an absolute reference point, however for a

semiconductor this is not a good absolute measure. Instead peaks with, from literature, well-known absolute energy position and that in addition are chemically stable under the present processing conditions has been used. Most often the choice has been Au *4f* or Si *2p* as reference point and the distance between those peaks and the peak of interest (e.g. As *3d* or Ga *3d*) has been measured.

### 3.3.2. Description of the atom in an XPS context

In order to explain some of the terms used in section 3.11 and to be able to further discuss the analysis and data treatment I will now give a very brief overview of the atom in the context relevant to XPS.

The electrons in the atoms in a solid are either *core electrons*, closely bound to the atom nucleus and found in the fully filled inner shells of the atom or valence electrons, more loosely bound found in the partially filled outermost shell of the atom.

The core level electrons are not participating in chemical bonds in a material. However, their binding energy is anyway affected by its chemical surrounding and the overall charge of the atom. Consequently an As-atom bound to a Ga-atom will have a binding energy different from an As-atom bound to oxygen and hence give rise to different peaks as can be seen in Figure 3.12. This shift in binding energy within the same core-level is called *chemical shifts* and they can give important information about the chemical composition of the sample surface.

The valence electrons are the electrons contributing to the chemical bonding between the atoms in a solid material. The valence electrons in a semiconductor are shared between neighbouring atoms. Since they are so loosely bound they are not quantized but there is instead a band of available energy states that they can occupy.

Each orbital in an atom can be completely described by its energy, angular momentum and a vector component of the angular momentum (the magnetic quantum number). These three properties are represented by a set of *quantum* numbers; $n$, $l$ and $m$ respectively that are related to each other. In addition each orbital can be occupied by only two electrons, one with spin up and one with spin down (represented by quantum number $s = \pm 1/2$). The first few values of the quantum number $l$ ($l$ = 0, 1, 2, 3, $n$-1) is historically described by the letters *s*, *p*, *d* and *f* and together with the energy quantum number $n$ we use them to describe the *electron configuration* of atoms. This is why XPS core level spectra are denoted by for example As *3d* where $n = 3$ and $l = 2\ or\ d$.

An electron always has a spin. If in addition it also occupies an orbital with some angular momentum (e. g. if $l$ is larger than 0) a coupling between the magnetic

field arising from the electron spin and its angular momentum will occur. The total angular momentum is described by $j = |l \pm s|$. For electrons in orbitals higher than $s$ this means that the energy level will be split into two different energy levels. This is called *spin-orbit splitting* and shows up in XPS spectra as two peaks instead of one. Consequently during data analysis these peaks are fitted using two components. The blue and the green peaks in Figure 3.12 are both *doublets* meaning that they are each a convolution of two components.

The value of the branching ratio (e. g. the relative size of the two components in the doublet) is also determined by the quantum numbers. It should be 0.667 in a *3d* shell. The quantum number is $n = 3, l = 2, s = \pm 1/2$ and hence $j = 5/2$ *and* $j = 3/2$. The *3d* shell has a total of 5 orbitals (from $-l$ to $l$ often denoted $ml = -2, -1, 0, 1, 2$) which can hold a total of 10 electrons; 2 in each orbital, one with spin up and one with spin down. Among the 10 electrons 4 can be found in the $j = 5/2$ and 6 in the $j = 3/2$ (from $-j$ to $j$ often denoted $mj = (-5/2), -3/2, -1/2, 1/2, 3/2, (5/2)$). This gives the relation $4/6 = 0.667$ which is indeed the branching ratio found for a *3d* orbital.

### 3.3.3. Analysis and fitting of XPS data

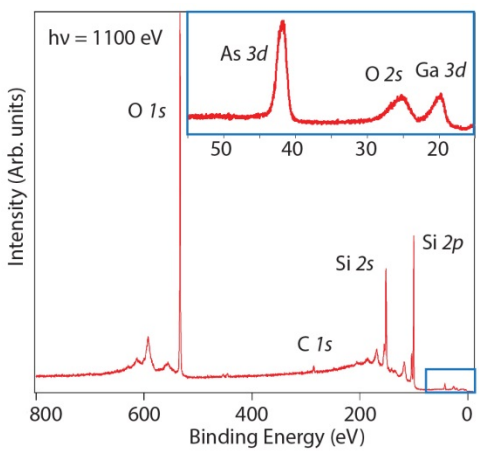


**FIGURE 3.11**
XPS overview spectrum of a Si substrate with deposited GaAs nanowires. The dominating peaks, O and Si, arise from the substrate. There are also some C contamination from the substrate. The nanowire footprint is shown in the inset. Since the nanowires only cover a small percentage of the surface, the signal from the Si and O of the substrate are much larger. (adapted from **paper I**)

An overview spectrum with low resolution covering a wide range of energies is often taken at the start of a new experiment. It provides evidence to which elements are present in the current sample. Example of such an overview is given

in Figure 3.11. For higher resolution the energy range and the step size is decreased (and often the acquisition time is increased) resulting in spectra as in Figure 3.12. Then, not only the involved elements but also their chemical states can be determined by a more detailed analysis. This is because the binding energy of the core levels is affected by the electronic and chemical surrounding of the atom from which the electron was excited. Importantly, the peak intensity is proportional to the amount of material present at the surface so the peak intensity also gives a measure of the relative concentration of any given species. The intensity also depends on the scattering cross section and losses due to inelastic scattering, but these can be accounted for. It induces extra information or will in some cases cancel out in relative comparisons.

The peaks of the elastically scattered electrons used to give chemical and elemental information can be modelled or fitted with specific functionals. Often the peaks are assumed to be a convolution of a Gaussian part and a Lorentzian part, commonly known as a Voigt function. Gaussian contributions arise from instrumental uncertainties and lattice vibrations. In Figure 3.12 is an example of a peak fitted with two doublets.

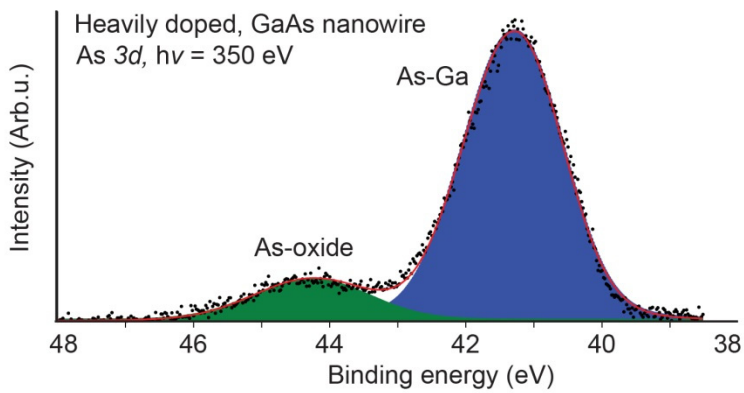


**FIGURE 3.12**
XPS of the As *3d* core level peak, accquired with a photon energy of 350 eV. The sample is GaAs nanowires heavily doped with Zn and deposited on a Si substrate. The spectrum is fitted with two doublets where we attribute the blue one to As bound to Ga and the green doublet to As-oxides. (adapted from **paper I**)

The life-time of the hole, that is left behind after an electron has been excited by the impinging photon and escaped its core level, gives rise to a broadening which is usually assumed to be Lorentzian by nature[73]. This broadening is core level specific and should be the same for all peaks arising from the same system.

The background at any given point arises from the inelastic scattered electrons, and while the specific distribution can be complicated to derive it is generally much smoother than the core-level peaks.

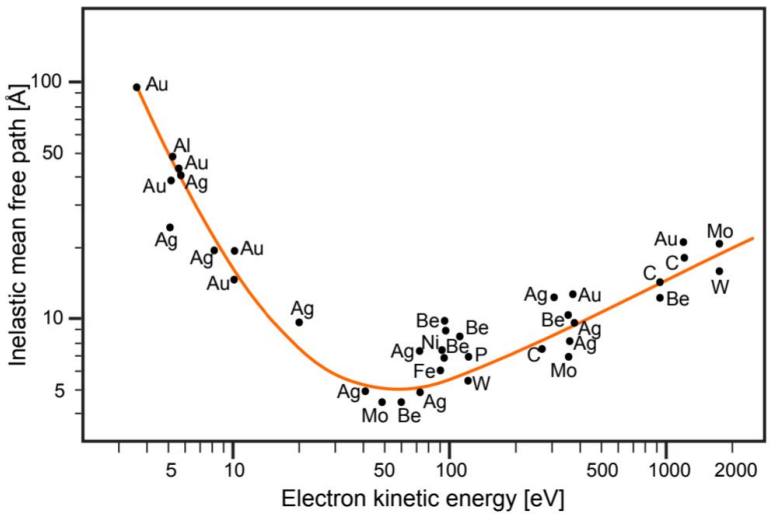


**FIGURE 3.13**
The universal curve. The inelastic mean free path in various materials of electrons at kinetic energies ranging between 0 and 2000 eV is shown. (adapted from [74])

The inelastic mean free path (IMFP) of a material or a gas is defined as the distance an electron beam can travel before its signal is reduced to 1/e due to inelastic scattering events. The mean free path is usually plotted against the electron kinetic energy in a curve commonly referred to as the universal curve (Figure 3.13). Checking for the kinetic energies used in soft-X-ray techniques (e.g. < 3 keV) it can be observed that the IMFP for these kinetic energies is between a few and a few tenths of Ångström. The electrons escaping the sample and getting detected must therefore originate from the top few atomic layers of the sample. An advantage of this is that it makes XPS a very surface sensitive technique and that by varying the photon energy or incidence angle the distribution of chemical species at the surface can be derived.

A disadvantage of the high inelastic scattering rates of electrons is that the pressure at where we can usually perform XPS is extremely low, limited to UHV, since at higher pressure the electrons will collide with gas molecules before reaching the detector. This is limiting since it is not always possible to extrapolate the result of a reaction in ambient condition from one in UHV. The discrepancy in what pressures we can measure in and what pressures we would like to measure in is known as the “pressure gap”. A lot of effort has been aimed towards bridging

the pressure gap and one progress is the development of high-pressure XPS (HP-XPS). Using special instrumentation with differential pumping and several lenses it is possible to perform measurements in the mbar regime which is much closer to realistic pressures for many interesting reactions. In **paper V** we present the result of HP-XPS measurements of the reaction of the first cycle of ALD of $HfO_2$ on InAs.

### 3.3.4. Synchrotron radiation

During the 1970s another, even more effective ways of generating X-rays was developed, i.e. the large synchrotron rings. In a synchrotron electrons are accelerated to energies in the MeV regime.

**Synchrotron**

- Storage ring.
- Electron gun.
- Electron accelerator.
- Bending magnets.
- Insertion devices.

A fundamental property of a charged particle, accelerated to quasi-relativistic speeds, is that when its trajectory is changed it will eject highly energetic electromagnetic waves normal to its path. This is utilized in a synchrotron. The trajectories of the electrons accelerated to high energies are bent by an assembly of magnets resulting in the ejection of electromagnetic waves. Various insertion devices such as wigglers and undulators are used to enhance this effect by guiding the electrons through a wave motion due to the alternating magnetic fields resulting in the emittance of X-rays with high intensity at specific wavelengths depending on the configuration of the linear magnetic field lattice which can be controlled by the user. This electromagnetic radiation is used to examine a large variety of samples in various different ways. Depending on the energy of the light we talk about “soft” X-rays in the energy range 0-3000 eV or “hard” X-rays in the energy range 3 - 30 keV.

During my years as a PhD student I have had the great privilege to perform all my XPS experiments at various synchrotron facilities around Europe. A synchrotron offers great advantages over a lab source such as a high photon flux, a possibility to change the photon energy and as a result a great flexibility of the instrument as for example in the application of high-pressure XPS described in 3.3.3.

The experiments described in **paper I** was performed at the beamline i311 at MAX II (now moved and upgraded to MAX IV) in Sweden[75]. I311 was a soft X-ray, undulator beamline with an energy range of 30-1500 eV. The spot size on the sample was 0.5 mm x 0.1 mm and it had a Scienta SES200 electron energy analyzer enabling high-resolution XPS[76].

The experiments performed on the GaSb flat substrates and nanowires (**paper III**) were conducted at the beamline SUPERESCA at Elettra Sincrotrone in Italy. SUPERESCA is also a soft X-ray, undulator beamline offering an energy range of 90-1500 eV. The spot size is 0.1 x 0.15 mm and the beamline has an in house developed 1D detector.

## 3.4. Small Angle X-ray Scattering

Another X-ray technique is Small Angle X-ray Scattering (SAXS). It was used during the work of characterizing Au seed particles of the aerotaxy nanowires in **paper VI.** I was mostly involved in the development of the set-up and performing the initial SAXS measurements of diluted aerosols. Therefore I give just a brief description of the principles and not further details that go beyond these measurements.

SAXS is, in contrast to XPS, an X-ray in X-ray out scattering technique. X-rays with higher energy (typically in the range 8-20 keV[77] are used and we detect the elastically scattered x-rays rather than the escaping electrons as in XPS.

SAXS is performed in transmission mode where the X-rays are shot through the sample under investigation and the scattering at small angles around the directly transmitted beam is detected. The SAXS set-up is described in Figure 3.14. X-rays are directed through the flow of nanoparticles and the nanoparticles will scatter the X-rays. However, some of the X-rays scatter only a very small angle. The very small distances in reciprocal space represent large distance order and periodicity in real space. These are the scattered X-rays detected in SAXS. Therefore, using SAXS it is possible to gain information about the size and the shape of the particles under investigation if their sizes are in the nanometer range[78].

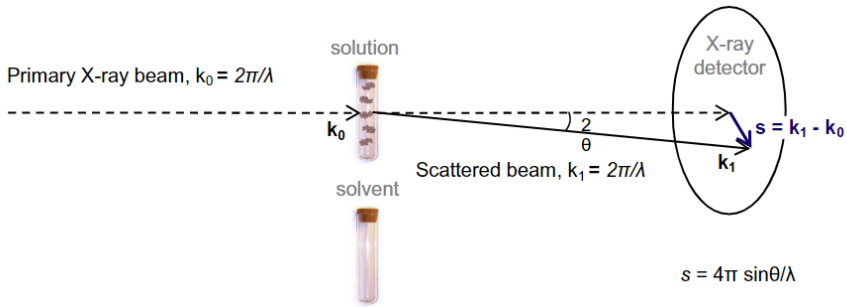


**FIGURE 3.14**
Schematics of a SAXS set-up. A focused beam of X-rays is directed onto a sample. In the figure seen as a capillary with solution but in our experiment, in paper VI, a tube with flowing nanoparticles. X-rays scattered by a small angle is detected. (adapted from [78]).

# 4. Characterization of and with nanowires

In chapter 4 I present a description of the experiments done in this thesis. I start in section 4.1 by presenting results connecting to cleaning and passivation of surfaces which has been the main concern of **paper III**, **paper IV** and **paper V**. I dedicate section 4.2 to studies related to aerotaxy nanowires, both surface studies (**paper I**) and *in-situ* studies (**paper VI**) of their seed particles. Finally in section 4.3 I give a detailed description of the development, production and use of GaN nanowires as probes for SPM (**paper II**).

A semiconductor-oxide interface is needed for many electronic devices, for example MOSFETs. During the era of Si and $SiO_2$ this interface was quite early perfected to a high level with an extreme minimization of defects and is now close to perfect. For III-V semiconductors it is different since the semiconductor-oxide interface contains a lot of defects. Therefore much of our efforts aim towards removing the native oxides to develop defect free interfaces and surfaces of III-V semiconductors, first for planar substrates, and later also for nanowire surfaces.

Furthermore, miniaturization of devices requires oxides with high dielectric constant, which nowadays are deposited with atomic-layer control by ALD. For III-V surfaces the ALD process comes with the additional advantage of a *self-cleaning* effect. This effect is not yet perfect or fully understood but it is resulting in a reduction of native oxides.

For InAs there are still issues with remaining defects and incomplete ALD. To better understand the process *in-situ,* time-resolved, study of the surface chemistry was needed which motivated the research presented in **paper V**. In section 4.1.1 I present the results of our studies of the interface between InAs and $HfO_2$.

For GaSb it is even more difficult, as the self-cleaning effect is insufficient (incomplete). In that case separate native oxide removal prior to the high-*k* ALD

was needed. This is what we address in section 4.1.2 where we explore the oxide reduction on GaSb using H-plasma cleaning. The preliminary results are presented in the manuscript of **paper III**.

Studies of the surfaces of aerotaxy nanowires are presented in section 4.2.1. Here we completely focus on oxidized nanowires. We examine the effect of Zn doping on the surface morphology and composition and find that the Zn, at very high doping levels, can protect the nanowire from detrimental native surface oxides forming in air (**paper I**).

Also for the GaN nanowire probes, presented in section 4.3, the oxidation is an important question. For SPM studies GaN offers great advantage in the formation of only a very thin oxide in ambient conditions. The (almost) lack of surface oxides allows to skip the cleaning process, shortening and simplifying the probe fabrication (**paper II**).

# 4.1. Surface cleaning and passivation

The structural quality of the interface directly influences the conductivity and device performance. During device fabrication unwanted atomic scale defects are introduced. One such defect is oxides resulting in high interface trap densities. In this section I present different studies of cleaning of surface oxides.

## 4.1.1. Cleaning of InAs

The atomic layer deposition of ultra-thin, high-*k*, oxide barriers offers self-cleaning and substitution of the detrimental native oxides forming on InAs in air. The effect is not yet fully understood. One reason for the lack of understanding is that most surface studies have previously been performed on the surfaces *after* ALD. Studies of the process *in-situ* or detailed studies of each step of surface treatment were still lacking. In **paper IV** and **paper V** this was addressed.

In **paper IV** several important steps of surface treatment of an InAs sample were studied. This study was initiated since other studies[79] indicated that thermal oxidation before the ALD step would significantly improve the device. XPS was performed on the sample (i) before any treatment, (ii) after atomic H-cleaning, (iii) after thermal oxidation in UHV, (iv) after exposing the sample to air again and finally (v) after $Al_2O_3$ ALD on the sample again. XPS core level spectra from the first three of these steps are shown in Figure 4.1 (a)-(f). To briefly follow up on this let us explore the effects of introducing a thermal oxidation layer after H-cleaning but before ALD of the high-*k* oxide.

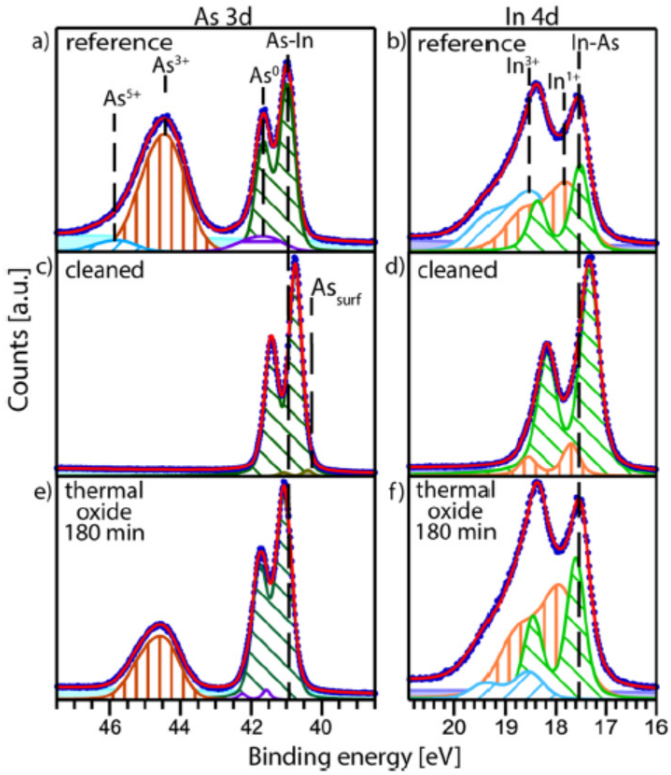


**FIGURE 4.1**
XPS data showing the core level As *3d* peak and In *4d* peak of an InAs flat substrate. (a)-(b) are reference spectra from before cleaning. (c) H-cleaning results in a complete reduction of the As oxides and (d) a reduction of the detrimental In $^{3+}$ oxides. (e)-(f) a thermal oxide on the samples after cleaning. The fitted doublets are marked in the figure. (adapted from **paper IV**)

In Figure 4.1 (a)-(b) we find spectra of the oxidized reference sample. H-cleaning is found to completely remove the As-oxides (Figure 4.1 (c)-(d)). The addition of a thermal oxide is shown in spectra in Figure 4.1 (e)-(f) where it can be seen that the oxide is different from the native oxides in Figure 4.1 (a)-(b). The process slightly improves the device which shows a decreased interface trap density observed via multi-frequency capacitance-voltage characterization. More interestingly the stoichiometry of the InAs oxides forming during the thermal oxidation was different from the stoichiometry of the native oxides. This gives a clue to that it can be the stoichiometry of the oxide that is the cause of observed device improvement of the same samples. The thermal oxides were not stable when taken out of UHV conditions but seemed to revert to the stoichiometry of the native oxides. So even if improvement of the device has been observed through the thermal oxide, this must be small effects due to the reforming of the surface oxides.

In **paper V** we examine the ALD of $HfO_2$ on InAs and perform time resolved studies of the chemical interaction happening in the formation of the very first deposition cycle. The first deposition (half-)cycle is interesting as this is when the majority of the self-cleaning takes place.

By mimicking the conditions under which ALD is performed it was possible to form a better understanding of the interaction during the very first steps of ALD. This demand the use of HP-XPS since the ALD process is performed under higher pressures than what is feasible for ordinary XPS. In HP-XPS differential pumping and additional lenses are used to allow for measurements in higher pressures (mbar regime). Moreover, the set-up used for HP-XPS also allowed for XPS in UHV after the reactions. This was used to confirm the presence of a $HfO_2$ film and to show that the end result was fully comparable to commercially available ALD deposited films.

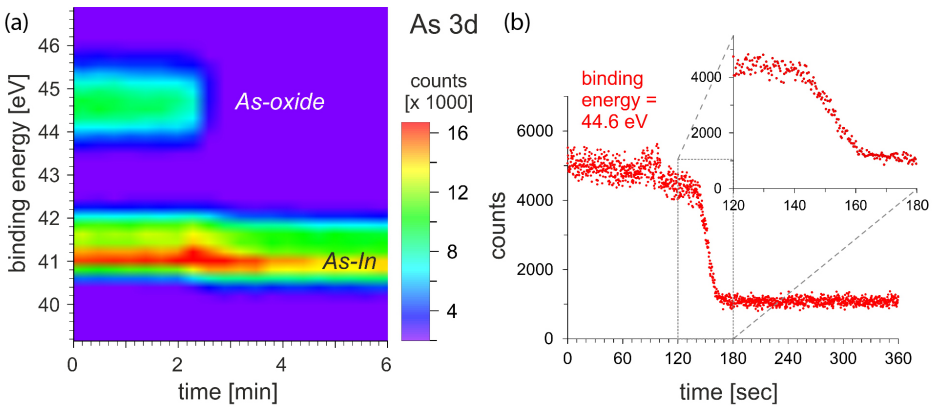


**FIGURE 4.2**
(a) Time-resolved XPS of the core level As *3d* peak of an InAs flat substrate during ALD showing the removal of the native arsenic oxides. The bulk peak as well as the oxide peak are marked in the figure. (b) Time-resolved evolution of the As-oxide XPS peak intensity at a binding energy of 44.6 eV during the ALD. The inset shows the timespan during which the reduction takes place. (adapted from **paper V**)

In Figure 4.2 the time resolved removal of As-oxides during the first half-cycle is shown. The peak intensity, plotted in Figure 4.2 (b), shows that the removal of the oxides is not instantaneous but happens over a time period of one minute. Additionally a shift in binding energy of the As-oxide peak was observed. The shift indicates that As-oxides in higher oxidation states are removed first followed by As-oxides in lower oxidation steps. Hence the native oxide removal is neither instantaneous nor homogeneous.

During the first half cycle of TDMAHf deposition it is interesting to note that the Hf-oxide formation (Figure 4.3 (b)) starts after the removal of the native oxides (Figure 4.2 (a)). This means that it is not, as previously stipulated, the formation of

the high-*k* oxides that is controlling the self-cleaning effect but rather the molecular adsorption of the precursors happening before.

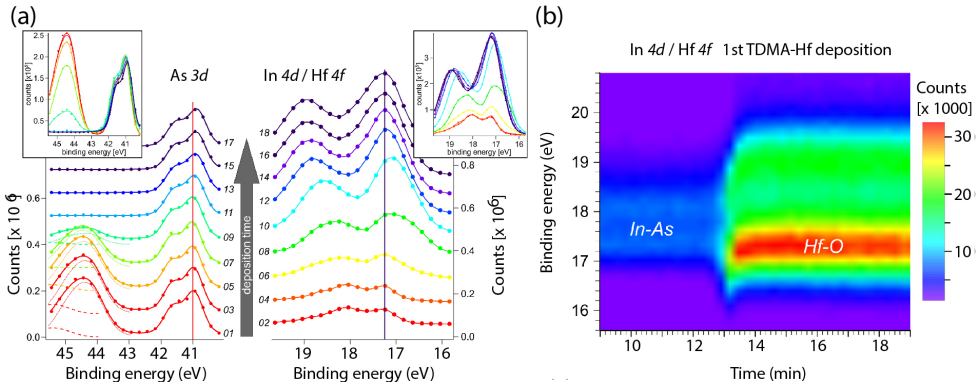


**FIGURE 4.3**
XPS core level spectra of (a) As *3d* and In *4d*/Hf *4f* peaks monitored during the first half cycle of ALD. The filled circles shows data points while the dashed lines in shows the fitted components. (b) Time-resolved XPS of the In *4d*/Hf *4f* spectra. A shift in binding energy is observed right before the formation of Hf-oxides. (adapted from **paper V**)

Turning to Figure 4.3 another interesting observation is a sudden shift in binding energy of the In *4d*/Hf *4f* that happens right before the formation of Hf-oxides. This shift is explained by a chemisorption step, not present in the current simplified description of ideal ALD. The studies performed here suggest not only the need for a revision of the description of the ALD but also that the length of the precursor pulses can affect the completeness of the oxide removal.

### 4.1.2. Cleaning of GaSb wafers and nanowire surfaces

Devices such as field effect transistors and tunneling diodes in a metal-oxide-semiconductor configuration has been realized with InAs nanowires[80]. Using GaSb, with its high hole mobility, it is possible to extend this to a complementary metal-oxide-semiconductor geometry[81] and nanowire heterostructures of InAs-GaSb has already been actualized[82,83].

The main challenge with implementing GaSb into devices is its unideal surface with an excess of surface states partly originating from a high density of defects and a continuously growing native oxide that is not self-limiting. The Ga- and Sb-oxides are also more difficult to remove compared to e.g. In- and As-oxides. Promising attempts to remove these oxides has recently been conducted using $N_2$ and $H_2$ plasma resulting in an interface with a significantly decreased density of states[84]. Here we have studied the cleaning of GaSb flat substrates and nanowires using H-plasma.

To generate the H-plasma a Tectra gen 2 plasma source was used. The samples were cleaned during a total of 20 minutes. The cleaning was interrupted and spectra were taken after 2 minutes, 10 minutes and finally after 20 minutes. In Figure 4.4 and Figure 4.5 the strong reduction of Sb-oxides and Ga-oxides on a GaSb flat substrate as well as on nanowires using H-plasma cleaning is shown.

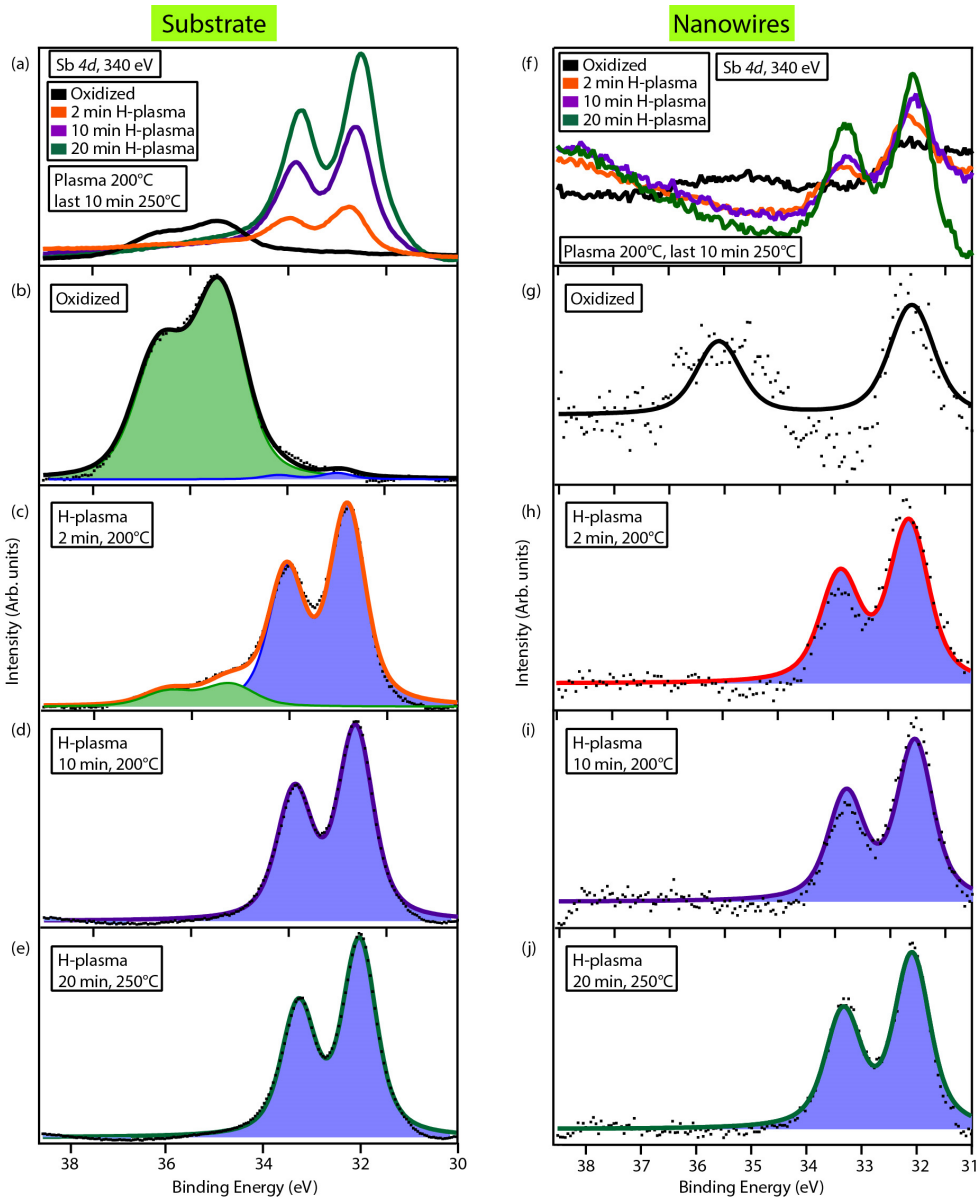


**FIGURE 4.4**
XPS of the Sb *4d* peak of (a)-(e) a GaSb flat substrate and (f)-(j) nanowire sample during H-plasma cleaning. (a) and (f) shows a comparison of the spectra acquired at different times of cleaning. (b) and (g) shows the oxidized samples, (c) and (h) shows the oxide reduction after 2 minutes of cleaning, (d) and (i) after 10 minutes of cleaning and finally (e) and (j) after 20 minutes of cleaning. Spectra from the oxidized substrate sample (black line) and after 2 minutes of cleaning (orange lines) are fitted with two doublets, one for Sb bound to Ga (blue) and one for Sb bound to oxygen (green). Spectra after 10 minutes (purple lines) and 20 mminutes (dark green lines) are fitted with one doublet for the Sb bound to Ga.

We first turn to the oxide reduction observed in the Sb *4d* spectra (Figure 4.4). The oxide is fitted with one doublet (green) and Sb bound to Ga (blue) with another one. It is clear that already after 2 minutes of cleaning the oxide is reduced considerably for the substrate and completely for the nanowires. For the oxidized nanowire sample (Figure 4.4 (g)) the intensity is low and it is difficult to obtain an unambiguous fit. Therefore it is currently fitted with two peaks, separated by 3.5 eV.

The same trend is observed for the Ga-oxides though the Ga oxides are tougher to reduce (Figure 4.5). The oxidation is observed to be less dominating for the nanowires than for the substrate. Several doublets were required to fit the Ga *3d* spectra. We attribute the green doublet to $Ga_2O$, the yellow doublet to $Ga_2O_3$ and the red doublet to a mixed oxide, such as $GaSbO_4$.

After 2 minutes of cleaning the Sb oxides are significantly reduced while at the same time the $Ga_2O$ peak grows. This we attribute to the Ga-Sb-O redox which has been observed previously[85,86].

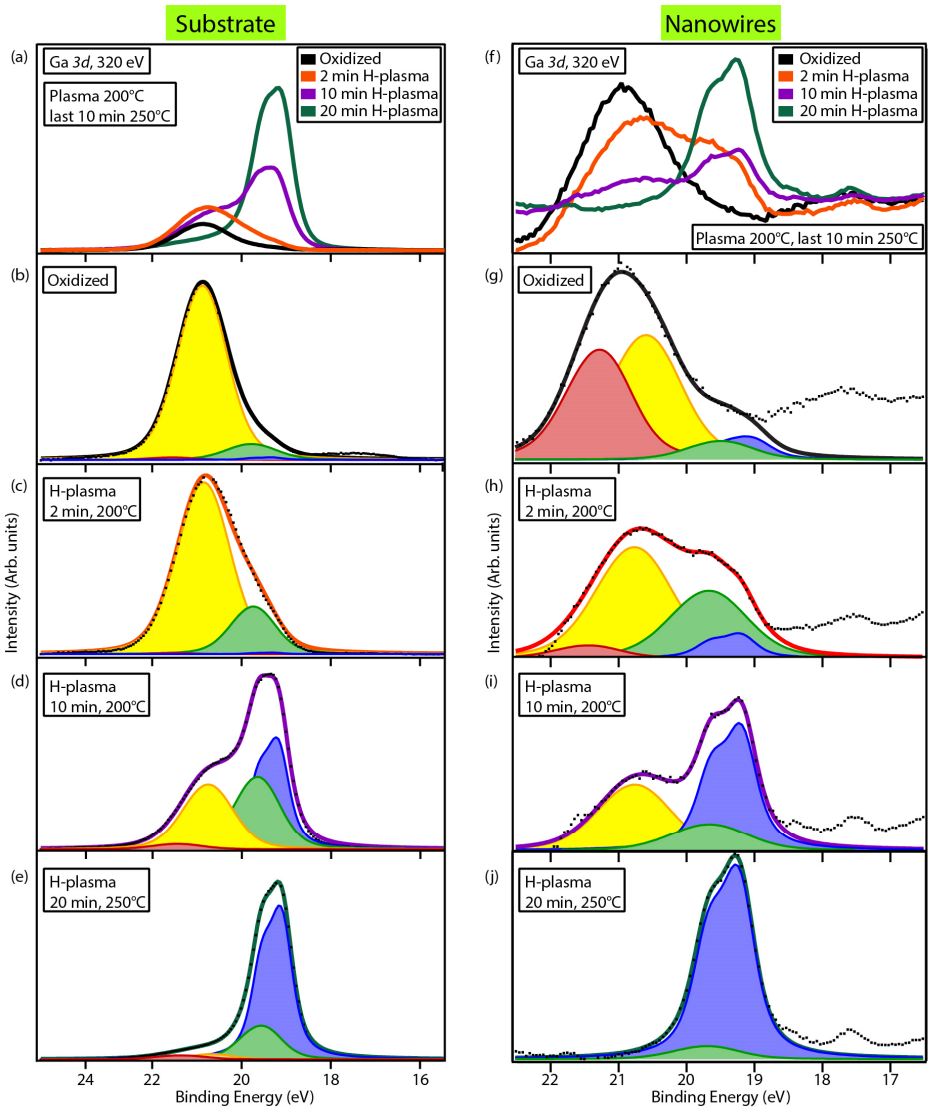


**FIGURE 4.5**
Ga *3d* peak of GaSb flat substrates and nanowires during H-plasma cleaning. The cleaning results in a strong reduction of the Ga native oxides on both (a)-(e) flat substrates as well as on (f)-(j) nanowires surfaces. All spectra are fitted with four doublets; 3 different oxide species (red, yellow and green) and one doublet corresponding to the Ga bound to Sb (blue).

This study shows that prolonged H-plasma cleaning, at as low temperature as 250° C, can completely remove all Sb-oxides and potentially remove all Ga-oxides. In our case we are left with a small amount of the less detrimental Ga-oxide $Ga_2O$. We suggest to incorporate H-plasma cleaning as a standard pre-treatment in plasma-enhanced ALD.

## 4.2. Aerotaxy nanowires

In aerotaxy the nanostructures are grown from aerosol seed particles in a gas flow. Growth by aerotaxy is still in an early stage and more research is needed to map both the growth process as well as characterizing the resulting nanostructures. Compared to other types of nanowire growth not much is known either about the aerotaxy nanowire surfaces and composition or about the synthesis and growth process. The growth process, conducted in gas phase, is technically vastly different from other nanowire growth processes and imposes new challenges in mapping and following of the growth step by step. Also the resulting nanowires differ from what we are used to characterize. Due to their different morphology, with a round cross-section and very small side facets, they become challenging for both cleaning and characterization by SPM compared to nanowires with large, flat side facets. We have tried to tackle these challenges and we have studied surfaces of GaAs nanowires grown by aerotaxy. This is presented hereafter and in **paper I**.

Additionally, we have used considerable effort to develop a way to perform *in-situ* SAXS studies, at synchrotron facilities, of the Au seed particles used for growth as they are dispersed in a gas flow. This is presented in section 4.2.2 and in **paper VI**.

### 4.2.1. Surface studies

The GaAs aerotaxy nanowires studied in **paper I** were grown using the precursors trimethylgallium (TMGa) for group III and arsine ($AsH_3$) for group V. At feasible temperature and TMGa/$AsH_3$ ratio the nanowires start to grow from the Au particle in the [111]-direction. During growth also diethyl-Zn (DEZn) was supplied to incorporate *p*-type Zn doping in the nanowires.

In **paper I** we compare aerotaxy GaAs nanowires with different amount of Zn doping. XPS is used to get an understanding of the elemental composition in the top layers of the nanowire surfaces and AFM is used to understand their morphology. The nanowires were *p*-doped with Zn to a DEZn/TMGa ratio (given in percent) of 3.5%, 60% and 100% and we denote these as lightly doped, medium doped and highly doped, respectively. The actual value of the incorporated dopants is not known.

The morphology of the nanowires is examined by SEM and AFM. SEM images of nanowires from the different growth batches are shown in Figure 4.6. Already from SEM images it is clear that the different doping ratios affect the growth of the nanowires. At a low doping the majority of the nanowires are still straight and uniform but for higher doping more nanowires start to look tapered and the growth also results in more debris. In Figure 4.6 (d) an AFM height image of a part of a

medium doped nanowire is shown. The Au particle is seen to the left in the image. The apparent width of the nanowire is exaggerated in the AFM image due to imaging artefacts. The true width of the nanowire should be closer to 150 nm as observed in the color bar on the right.

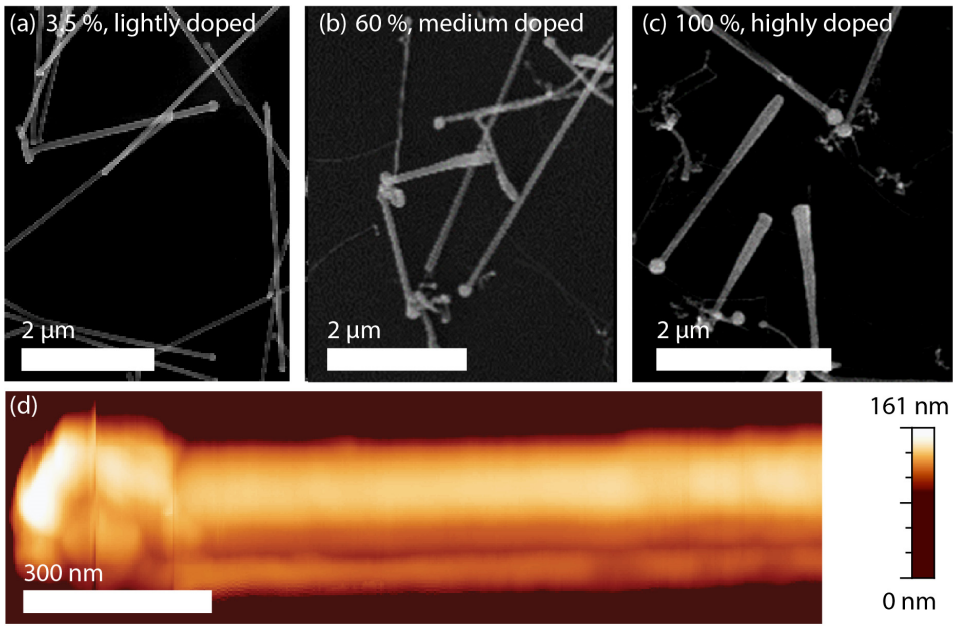


**FIGURE 4.6**
(a)-(c) SEM images of GaAs nanowires with different Zn doping. The growth ratio of DEZn/TMGa, is shown in percentage in each case. (a) shows lightly doped nanowires. (b) shows medium doped nanowires. Some of the nanowires are tapered and of varying thickness. (c) shows highly doped nanowires. At this doping the tapering is considerable and a lot of debris from the growth is present. (d) AFM image of a medium doped aerotaxy nanowire. (Adapted from **paper I**)

Using XPS we study the As *3d* and Ga *3d* core levels to get an understanding of the surface oxidation of the nanowires. Spectra with these core levels are shown in Figure 4.7. The As-oxides on the medium and highly doped samples are actually exceptionally low for an oxidized sample possibly indicating that the Zn might have formed a protective layer covering the nanowire. However, the amount of Zn detected on the nanowires using XPS indicates a maximum of 2 atomic layers on the highly doped sample and only a partial layer of Zn on the medium doped sample. This would mean that already a partial layer of Zn would protect the nanowire from oxidation for a time period of a couple of hours. A time frame like that would make a difference during device production as the nanowires could be transported between different growth and deposition systems without the formation of an oxide and thus facilitate the practical use of the nanowires.

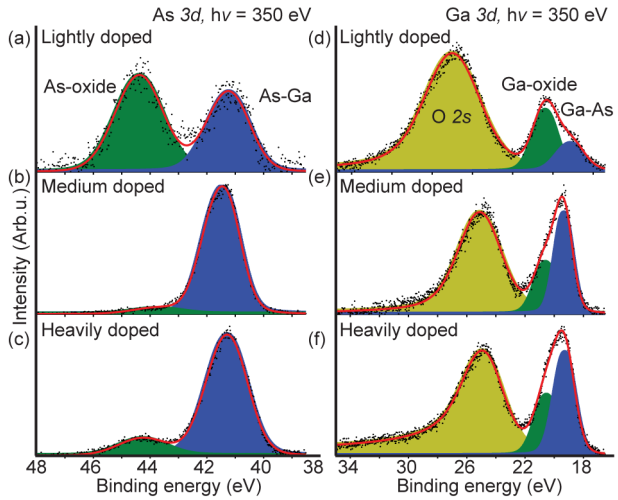


**FIGURE 4.7**
XPS of GaAs nanowires with different Zn doping. The XPS core level spectra for different nanowire dopings of (a)-(c) the As *3d* peak and (d)-(f) the Ga *3d* peak. The blue peaks are the fitted doublet of the bulk peak. The green peaks are the fitted oxides and the yellow peak shows the, with Ga *3d* overlapping, O *2s* core level peak. All spectra were aqcuired at a photon energy of 350 eV. (adapted from **paper I**)

Turning to the results of the AFM measurements we conclude that the Zn absorbed on the nanowire surface smoothens the surface morphology. The results are shown in Figure 4.8. The overall structure of the aerotaxy nanowires compared to their epitaxially grown counterparts is shown in Figure 4.8 (a)-(d). The aerotaxy grown nanowires exhibits a round cross section in contrast to the common hexagonal structure of the epitaxially grown ones meaning that the side facets are not large and flat but rather consist of a patchwork of smaller ones. Using STM on H-cleaned GaAs aerotaxy nanowires we have observed several small patches of unreconstructed {110} surface of approximately 5-10 $nm^2$.

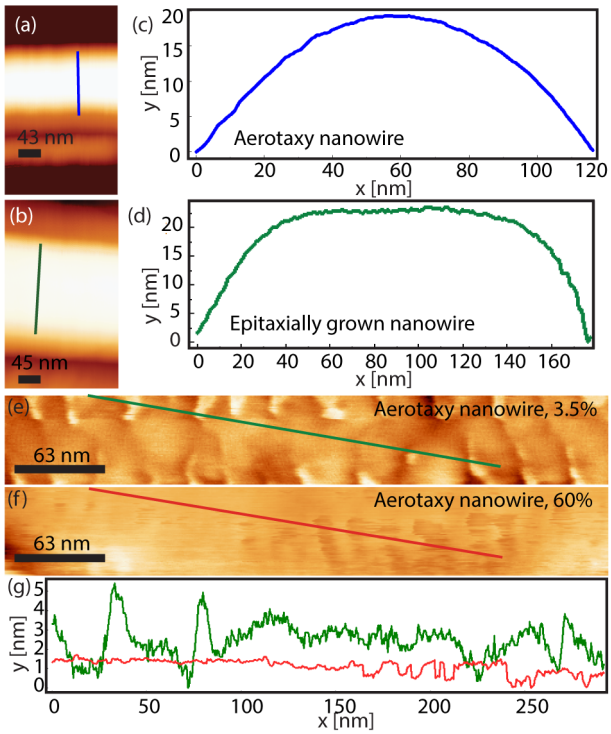


**FIGURE 4.8**
AFM height images of an (a) aerotaxy grown nanowire and (b) an epitaxially grown nanowire. Corresponding individual line scans marked, in the AFM images in (a) and (b), are displayed in (c) and (d) where the round cross section of the aerotaxy nanowire is compared to the hexagonal cross section of epitaxially grown nanowire. AFM height image of a (e) lightly doped and (f) medium doped nanowire surface with corresponding line scans in (g) showing the surface roughness ontop of the nanowires. (adapted from **paper I**)

### 4.2.2. *In-situ* studies

We have developed a technique to study heavily diluted aerosols in a gas flow. The particles we study are the seed particles used for aerotaxy growth. This is important in order to gain further control and understanding of the growth process of aerotaxy nanostructures and would be the first step towards full *in-situ* study of the entire growth process. To study dilute gases we need high X-ray intensities and thus the use of a synchrotron. Hence the complete seed particle generation system was moved to the European Synchrotron Radiation Facility as well as the MAX II synchrotron ring for development and demonstration.

The seed particles used for aerotaxy growth is generated using a spark generator in a flow of $N_2$ gas. Two electrodes are brought close together and a voltage is applied across them resulting in a spark kicking off material from the electrodes. The material is a distribution of particles with different size and shape. The

particles in the aerosol are sintered and size selected to obtain a more uniform particle aerosol and this process is depicted in Figure 4.9. The sintering is done by flowing the aerosol through a furnace melting the particles into spheres of different sizes. Two differential mobility analyzers (DMAs) are used to size select particles keeping only those of a desired size, usually between 5 and 100 nm.

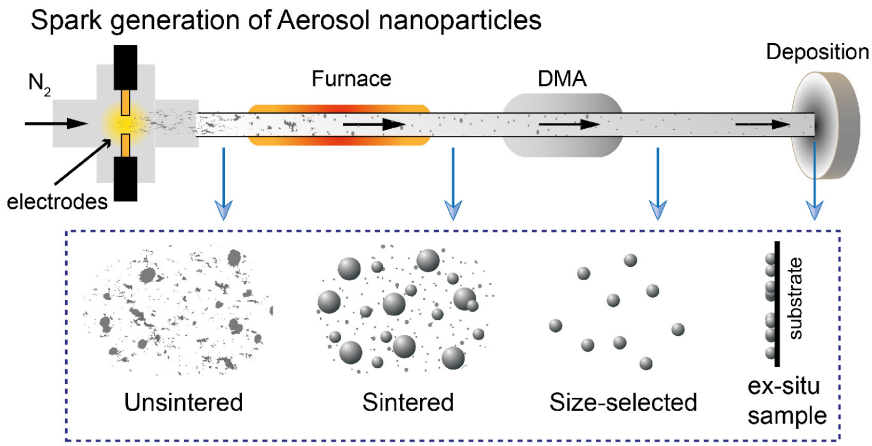


**FIGURE 4.9**
The set-up for producing an aerosol of nanoparticles. The particles are generated by a spark generator, sintered, size selected and finally deposited on a substrate. (adapted from **paper VI**)

The particles flow through the system carried by a $N_2$ gas. Our aim was to probe the aerosol at different stages of production in a manner depicted in Figure 4.9 and Figure 4.10. However, the volume fraction of the particles generated and measured before sintering was estimated to be $1 * 10^{-9}$ and after sintering $7 * 10^{-10}$ Earlier SAXS measurements have been successfully performed on volume fractions of down to $10^{-8}$ but our value is at least one order of magnitude lower than that. One viable option for ultra-dilute aerosols has been to deposit the particles before measuring them to achieve a higher concentration of particles. However, the particle-particle interaction as well as the particle-substrate interaction risks deforming the particles before being able to study them. Hence a development of the technique was needed.

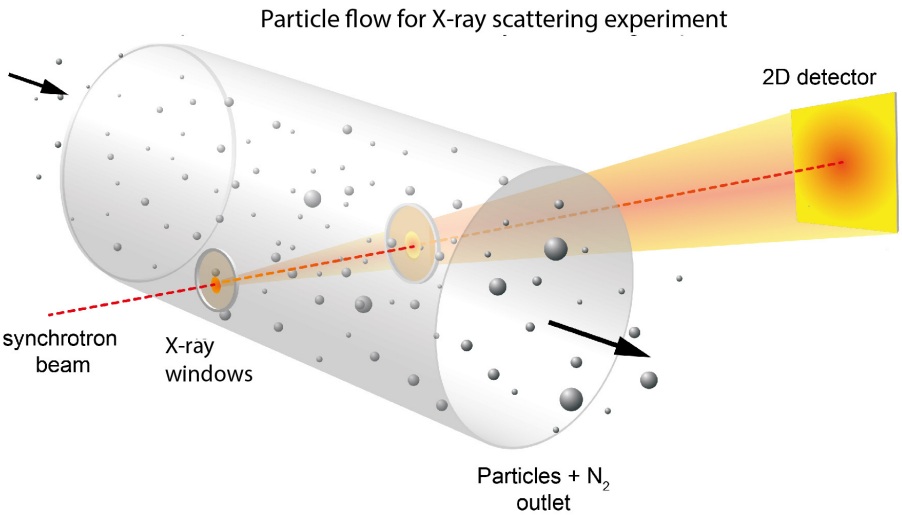


**FIGURE 4.10**
Schematic view of the particle flow during measurement of a dilute aerosol of Au nanoparticles. The X-ray windows were made of kapton and could be exchanged between each measurement for an increased accuracy of the background estimation. (adapted from **paper VI**)

The Au aerosol flow was measured after the spark generation when the amount of particles was observed to be the highest possible. Afterwards, we turn the particle generator off but let the system run until no more particles were detected. At this point we measure the background.

Since we already from the start had an extremely diluted aerosol to measure it was important to minimize the loss of particles between generation and measurement. To counter unnecessary particle losses we used a larger flow cell than normal to avoid turbulence and subsequent particle build-up on windows and internal walls. We also kept all tubing as short as possible to minimize particle losses to the tubing walls.

Another key to being able to measure ultra-dilute aerosols has been to carefully analyse and remove any background. During measurements we used thin kapton windows (depicted in Figure 4.10) for both entrance and exit point to minimize any loss of intensity of the X-ray beam. It was also beneficial to exchange the kapton windows to new, clean ones between every measurement. For the most demanding experiments we completely removed the windows and run the system on a slight under-pressure.

Lastly the method of data analysis has played an important role to extract the relevant data. More detail about the analysis methods used is found in **paper VI** but it is beyond the scope of this thesis.

## 4.3. GaN nanowire probes

STM and AFM have been invaluable tools for surface scientists for decades. Already in the early years of SPM the idea existed of developing tailor made probes. During the years, efforts have been made towards probes with specialized properties. Mapping of the luminescence while charge carriers are tunneling between the tip and the sample, was performed early on using a GaP tip[87]. This is now known as Scanning Tunneling Luminescence (STL). Furthermore, for STM, semiconducting materials such as InAs[88], ZnO[89] and diamond[90] have been successfully used.

We have developed a method of producing GaN nanowire probes for SPM. GaN nanowires have been used as probes for AFM[91] and SNOM[92] but our work is the first reported case where it is used for STM.

Using a nanomanipulator we place a single nanowire on the very tip of an existing probe. The process is shown in Figure 4.11. Arrays, as in Figure 4.11 (a), of GaN nanowires with very similar shape make just a single growth substrate enough for millions of tips. We pick up a single nanowire using a nanomanipulator inside an SEM. The nanowire is then carried to the tip of the SPM probe where it adheres to its surface. To create a better electrical contact between the nanowire and the tip we deposit Pt using the electron beam in the SEM. A nozzle, supplying the metal organic precursor (methylcyclopentadienyl trimethyl platinum), is inserted close to the sample. The electron beam cracks the gas molecules of the precursor resulting in deposition of Pt.

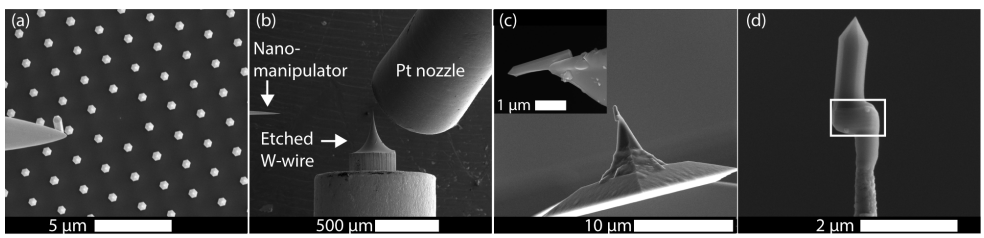


**FIGURE 4.11**
The procedure of making GaN single nanowire tips for STM and AFM. In (a) a single nanowire is picked up from its growth substrate using a nanomanipulator inside an SEM. The nanowire is then carried to the tip (b), placed at the very end of the probe and "glued" using EBID of Pt. Image (c) and inset shows a prepared AFM probe and (d) an STM probe. The area of Pt deposition is highlighted by a white rectangle in (d). (Adapted from **paper II**)

The method is versatile and in this manner we have put nanowires on several different substrates such as etched tungsten wires (**paper II**), commercial Pt probes, sapphire and GaAs wafers as well as on commercial AFM probes (**paper II** and Figure 4.12).

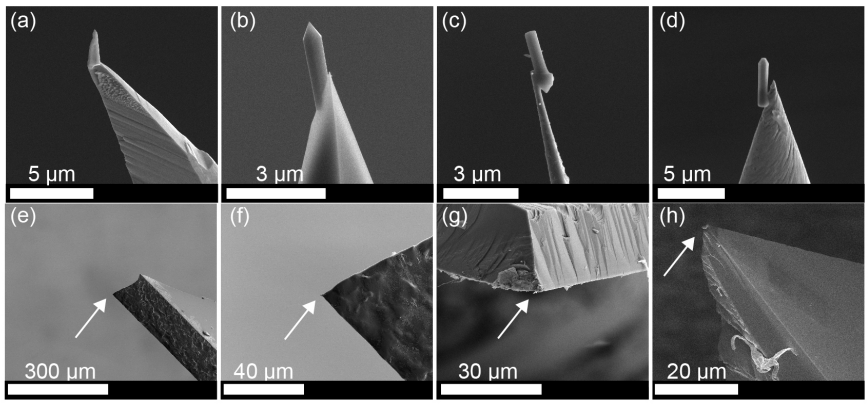


**FIGURE 4.12**
GaN nanowires mounted on different substrates and in different configurations. The SEM images shows GaN nanowires mounted on the following substrates: (a) W-wire after FIB treatment, (b) a commercial $SiO_2$ AFM probe, (c) a W-wire with the GaN nanowire in upside down configuration, (d) a Pt probe for STM, (e) a Si wafer ((f) zoomed in on (e)), (g) a GaAs wafer and (h) a sapphire wafer coated with Au. Arrows indicate the nanowire position in (e) to (h).

In the following sections I show results from the use of GaN nanowire probes for STM/S and AFM.

### 4.3.1. GaN nanowires as STM/S probes

In **paper II** we describe how we have developed a method to produce GaN nanowire probes for STM and AFM. In Figure 4.13 (a) the schematic of our GaN nanowire STM probe is shown. In this case we have used a gold plated omicron tip holder Figure 4.13 (b) and placed the nanowire on the etched W wire attached to it. The technique is not limited to a special kind of holder but will work with any STM holder.

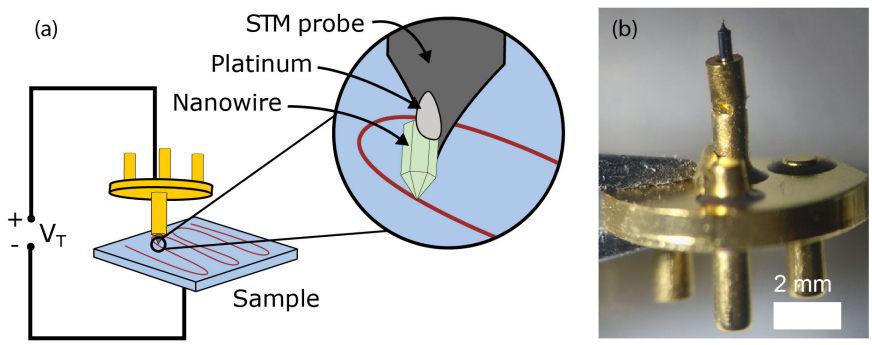


**FIGURE 4.13**
(a) Sketch of a GaN nanowire STM probe. The nanowire is placed on the W-probe and secured with EBID of Pt. (b) Picture of a GaN nanowire STM probe.

The idea of using nanowires as probes for STM is appealing for several reasons.

**GaN nanowire probes**

- Well-defined shape.
- Thin native oxide.
- High hardness.
- Large direct bandgap.
- Low X-ray optical density.
- Possibility of heterostructuring.

The nanowires have a well-defined and well-known shape. Since an STM image is always a convolution of the combined system of the tip and the sample there is a great advantage to know the shape of the tip to de-convolve the image and extract information about the sample under investigation.

The native oxide forming during ambient conditions on GaN is thin. The oxide is dominated by $Ga_2O_3$[93,94] and reportedly under one mono layer for a Ga-terminated (0001) surface[95] allowing us to conveniently tunnel through using STM. This means that we have the luxurious situation where we do not have to clean the GaN nanowire probes nor keep them stored under vacuum but can freely use them and transport them conveniently.

The hardness of GaN was recently found to be surprisingly high[96]. They are found at 7 on Mohs scale, on par with quartz and tungsten. GaN has a large, direct band gap of 3.4 eV[97]. It is also a material with low X-ray optical density meaning that it is transparent to X-rays opening up the possibility of simultaneous SPM and light experiments.

With the well-developed knowledge of GaN nanowire growth comes the possibility of heterostructuring[98] to further specialize the properties of the tips.

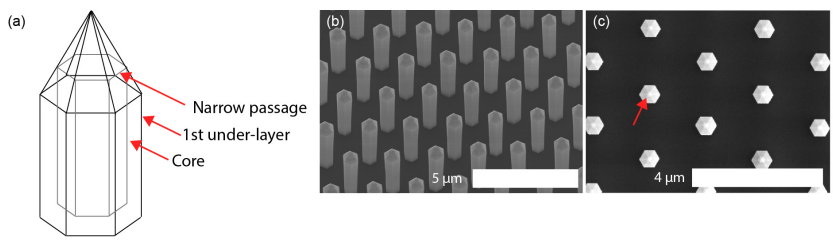


**FIGURE 4.14**
(a) A sketch showing a single underlayer nanowire. The (grey) core is covered by a (black) underlayer but the core is still cutting through the top side facets of the nanowire. (b)-(c) SEM image of GaN nanowires with a single underlayer. A red arrow in (c) marks the dark lines indicating the core visible in top view of the nanowires.

The structures are grown by selective-area epitaxy with metal-organic chemical vapor deposition (MOCVD). The growth is conducted in a three-step process in one growth run. During growth Si dopants are introduced to make the resulting nanowire *n*-type. A core, which has poor conductivity, is grown and covered by a radial underlayer of high quality GaN (as in Figure 4.14(a)). A second layer of high quality GaN is added to thicken the radial layer of conductive material and to make the sharp GaN tip tailored for SPM.

For a nanowire to be a well-functioning probe it has to be stable and conducting. In the first tries of using GaN nanowire probes a version of the nanowire was used that was grown using a two-step process as depicted in Figure 4.14 (a). This was not sufficient as the core, which is a poor conductor, cut through the tip structure (red arrow in Figure 4.14 (c)) creating an extremely narrow or no passage for the electrons to pass from the tip to the bottom of the nanowire which results in tip crashes on approach.

The band gap of the probe plays a significant role during STM/S. In case of a semiconducting probe on a metallic surface the situation is conceptually the same as if we use a metallic probe on a semiconducting surface. There is no inherent difference between a tip and a sample and the only thing to keep in mind is the sign and location of the applied bias. For a semiconducting probe on a semiconducting surface on the other hand we have some interesting things to consider.

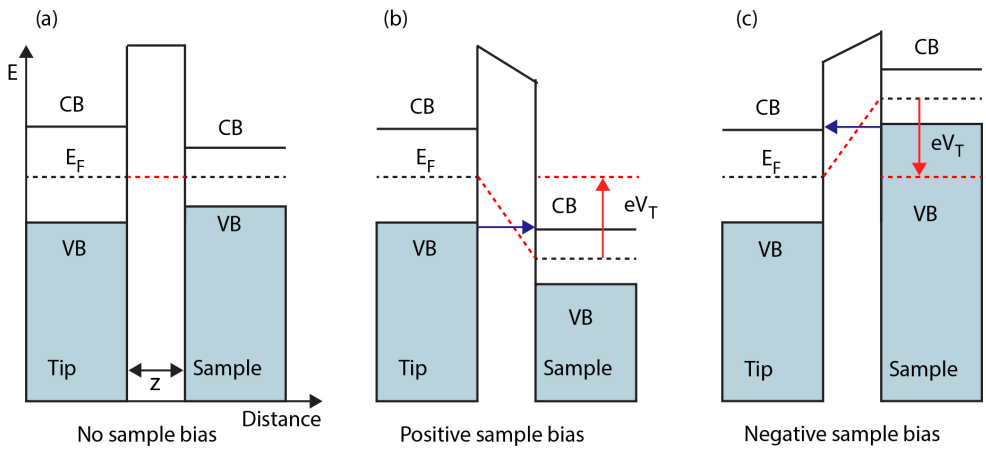


**FIGURE 4.15**
The band diagrams of an undoped semiconducting tip scanning on an undoped semiconducting sample. In (a) no bias is applied to the system. The band shifts realtive to each other when we apply a (b) positive or (c) negative bias to the sample. The conduction band (CB), valence band (VB) and the tip-sample separation (z) are marked in the figure. The Fermi level, $E_F$, is marked by a dotted black line. In the cases where a bias is applied over the system the difference in energy between the Fermi level of the tip and the sample is marked by $eV_T$ and indicated by a dotted red line and a red arrow.

Choosing appropriate parameters for approaching and scanning plays an important role in maintaining a long lifetime of the probes. For the scanning voltage one has to be sure to choose an energy that is outside of the combined band gaps of the tip and the sample which is the energy of two band gaps added together as can be seen from Figure 4.15. The position of the Fermi level is unknown, partly because the actual doping is unknown and partly because we might have tip induced band bending which would change the situation away from what is modelled in Figure 4.15. Therefore we commonly choose a value considerably greater than half of the combined gap which would otherwise be sufficient if the Fermi level was found in the middle of the gaps.

We have scanned various samples with the GaN nanowire probes. Here we present STM results from Au(111), GaAs(110) and InAs(111)B (e. g. the As-terminated surface). Common to all STM measurements with the GaN nanowire probes is that it has been proven difficult to obtain atomic resolution.

Scanning InAs(111)B we see the characteristic triangle shape islands (Figure 4.16 (a)-(b)) of the surface. By analysing single scan lines across the surface we can get an idea of the resolution.

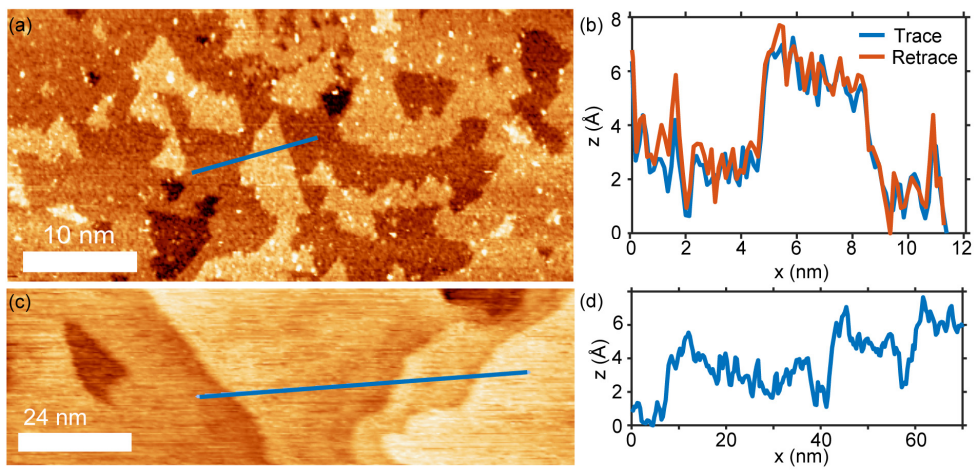


**FIGURE 4.16**
STM images acquired using a GaN nanowire probe. The scanned sample is in (a) an InAs(111)B sample with a tunneling current of I = 80 pA and a tunneling voltage of V = -4 V. (b) Line profile of both the trace (forward scan) and the retrace (backward scan) from the line marked in (a). (c) A Au(111) surface with (d) corresponding line scan. Scanning parameters on Au was a tunneling current of I = 40 pA and tunneling voltage of V = 3.5 V. (Adapted from **paper II**)

At a Au(111) surface (Figure 4.16 (c)-(d)) we obtain a similar resolution as we do on the InAs(111)B surface. The noise levels in both cases are 0.1 nm and on the InAs surface these electronic structures seem to be real as they appear in

individual scan lines back and forth on the surface. This could be electronic features arising from the interplay between the semiconducting tip and sample.

We can confirm the presence and function of the nanowire tip by imaging it with SEM before and after scanning. We can also confirm the presence of the nanowire on the tip using STS. So for example when performing STS on Au a clear bandgap is seen consistent with the presence of GaN.

### 4.3.2. GaN nanowires as AFM probes

GaN nanowires have been used as AFM probes before[91]. However, our probes are tailor made with a sharp tip apex and we show more extensive scanning results from atomic step scale to micron scale. Additionally, we developed a new preparation method that is quicker and more cost effective.

Our preparation method follows the same steps as the preparation of the STM probes but with a few minor differences. For AFM probe production we bring the entire cantilever chip into the SEM chamber. We pick up a nanowire from the growth sample using the nanomanipulator and transfer it to the AFM probe. We place the nanowire on the AFM tip. The commercial AFM tips we use have a pyramid shape. This means that the mounting will result in an angle of the nanowire with respect to the normal. This angle will affect the images acquired with the tip but can be accounted for in the image analysis.

We have scanned various samples with the GaN nanowire probes. Here we present AFM results from highly oriented pyrolytic graphite (HOPG) and $SiO_2$.

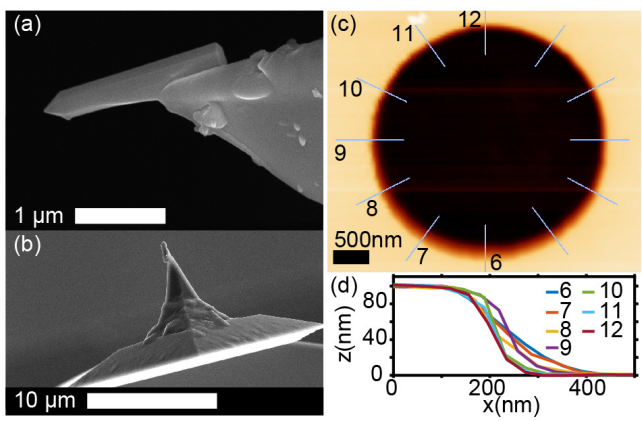


**FIGURE 4.17**
(a)-(b) SEM image of a GaN nanowire mounted on a commercial AFM tip. The pyramid shape of the AFM tip gives an inherent angle of the nanowire. (c) An AFM image of a $SiO_2$ test sample where a hole structure is imaged. (d) Line scans from the lines marked by numbers in (c). (Adapted from **paper II**)

All AFM images will be a convolution of the shape of the AFM probe and the scanned surface. Knowledge of the shape of the probe offers the opportunity to de-convolve the image and extract the part originating from the surface. This we do and describe in detail in **paper II** where we analyse the slope of the line scan when the probe enters or exits a hole in the $SiO_2$ test structure (Figure 4.17 (c)-(d)). Our results are comparable to earlier results of GaN AFM probes mounted differently[91].

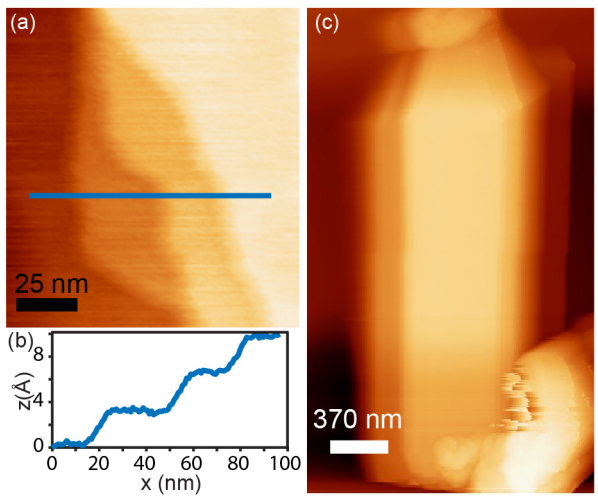


**FIGURE 4.18**
(a) An HOPG sample scanned with a GaN nanowire probe. (b) line scan of the line marked in (a) showing the atomic steps on the HOPG surface. (c) AFM image of a GaN nanowire imaged with a GaN nanowire probe.

Using a GaN nanowire probe we have scanned a HOPG sample. We can resolve atomic steps as shown in Figure 4.18 (a)-(b). We have also used a GaN nanowire probe to scan on a GaN nanowire and the result is shown in Figure 4.18 (c). The side facets of the GaN nanowire can be seen as well as the side facets of the pyramid tip structure.

# 5. Concluding remarks and outlook

In conclusion, focus has been on performing and developing characterization to resolve questions in three areas of III-V nanowire research; surface/interface quality, growth and applications.

First the technologically relevant interface between III-Vs and oxides has been investigated. Studies have been made on various III-V nanowire and substrate surfaces, such as GaAs, InAs and GaSb. The investigations of flat substrate surfaces can give more detailed information than what can be obtained from the confined nanowire surfaces which give only weak signals in for example XPS. As a result, the understanding gained from substrate surfaces is important in interpreting the nanowire results. Several different methods of surface chemical control have been investigated including atomic hydrogen cleaning, hydrogen plasma cleaning, thermal oxidation, Zn doping and self-cleaning by ALD. The surfaces of aerotaxy grown nanowires were investigated. The effect of Zn doping on the surface morphology and oxide was studied. It turns out that Zn doping might help with the passivation of aerotaxy nanowire surfaces – something that would allow for easier post-growth processing. Detailed studies of several critical steps of surface preparation were made on InAs. The effect of a thermal oxidation before ALD has been investigated. It is an approach that could open up for higher quality of the interfaces of devices. The thermal oxide showed a different stoichiometry than the detrimental native oxides. Though not stable in air some groups have still seen a positive effect on device performance. Using XPS and hydrogen plasma cleaning on GaSb substrates and nanowires we see a reduction of detrimental native surface oxides that goes further than what we have achieved with other cleaning techniques. The studies in this thesis show that there are many possibilities for improving the properties of the surface oxides on nanowires. However, it is also clear that much work remains in this area. One interesting avenue would be to directly combine the ultrahigh vacuum systems for cleaning and oxidation with an ALD system so that samples do not need to be transported in air. Going a step further one could even combine these directly with the growth systems. An alternative would be to follow up on effects as seen for the aerotaxy nanowires were a protective oxide is formed during initial synthesis which could allow transport. As the final aim is improved electrical/optical properties of the

nanowires it would also be interesting to couple the surface studies more directly with measurements of electrical and optical properties.

Second, the growth and synthesis processes are addressed *in-situ* with the development of the technique to study the seed particles of aerotaxy nanowires. Better knowledge of the yet, to a large extent, unknown processes behind aerotaxy growth is within reach as it is now possible to study each step of the growth *in-situ*. The developed technique is widely applicable to aerosols as well as other dilute systems to determine the reactive surface area of nanoparticles during different stages of their production or using different production schemes. This could be used also outside semiconductor industry of for example catalysis research, environmental studies or medical sciences. For InAs surfaces the ALD of $HfO_2$ was monitored *in-situ* using XPS. The discovery of the criticality of the adsorption step shows that there is a lot to learn using the new technique. Further experiments could be important for designing and optimizing ALD cycle parameters. Still only very few experiments have been performed and new studies on several more configurations of semiconductors and high-*k* oxides would be desirable to form a better general understanding in the area.

Third, one area of applications are found with the development of tools based on nanowires for further characterization and manipulation. In this context the thesis presents the creation of GaN nanowire probes with sharp tips. These probes have been shown to be useful for STM and AFM, but are not limited to these techniques. Interesting observations could be done using a large band gap semiconductor as an STS probe on semiconducting surfaces. The use of the large band gap and low optical density material GaN opens up to experiments with incorporated light and has potential use in scanning near-field optical microscopy. Already ongoing is the development of simultaneous STM/laser experiments using these probes. The advantageous structure of a nanowire also gives opportunities to use the probe as a wave guide guiding light onto or away from a sample. Further, their transparency to X-rays might prove useful when SPM is combined with X-ray imaging. Finally, I hope to see the precise GaN probe used in other applications, such as a nano-indentation tool, to make use of the hardness of the material.

In the future, one can imagine that the different approaches and methods presented in this thesis can be combined to improve our fundamental understanding of III-V nanowires as well as their function for applications. By combining the use of several in-situ X-ray methods both the synthesis and subsequent surface passivation/functionalisation can be followed “live” to get the complete picture of the nanowire when it is to be used in a device. SPM can then also be implemented to tell us exactly how the surface morphology is and tell us about electronic properties. Finally, the nanowires can be used as probes on themselves to obtain

better defined results as seen in Figure 4.18. The methods presented here are only a subset of what is used to study nanowires, and during the work for example various electron microscopies has also been of importance. In conclusion, only by combining many methods is it possible to gain a sufficient understanding of all aspects of III-V nanowires to allow them to fulfil their great promise in the coming generations of technology.

# Bibliography


[1] M. T. Deng, S. Vaitiekėnas, E. B. Hansen, J. Danon, M. Leijnse, K. Flensberg, J. Nygård, P. Krogstrup and C. M. Marcus, "Majorana Bound State in a Coupled Quantum-Dot Hybrid-Nanowire System", *Science* **354**, 1557 (2016).

[2] E. Hilner, U. Håkanson, L. E. Fröberg, M. Karlsson, P. Kratzer, E. Lundgren, L. Samuelson and A. Mikkelsen, "Direct Atomic Scale Imaging of III-V Nanowire Surfaces", *Nano Letters* **8**, 3978 (2008).

[3] X. Duan, Y. Huang, Y. Cui, J. Wang and C. M. Lieber, "Indium phosphide nanowires as building blocks for nanoscale electronic and optoelectronic devices", *Nature* **409**, 66 (2001).

[4] J. Wallentin, N. Anttu, D. Asoli, M. Huffman, I. Åberg, M. H. Magnusson, G. Siefer, P. Fuss-Kailuweit, F. Dimroth, B. Witzigmann, H. Q. Xu, L. Samuelson, K. Deppert, M. T. Borgström, "InP nanowire array solar cells achieving 13.8% efficiency by exceeding the ray optics limit", *Science* **339**, 1057 (2013).

[5] E. D. Minot, F. Kelkensberg, M.Van Kouwen, J. A. Van Dam, L. P. Kouwenhoven, V. Zwiller, M. T. Borgström, O. Wunnicke, M. A. Verheijen and E. P. Bakkers, "Single quantum dot nanowire LEDs", *Nano letters* **7**, 367 (2007).

[6] J. Bao, M. A. Zimmler, F. Capasso, X. Wang and Z. F. Ren, "Broadband ZnO single-nanowire light-emitting diode", *Nano letters* **6**, 1719 (2006).

[7] H. Riel, L.-E. Wernersson, M. Hong and J. A. Del Alamo, "III–V compound semiconductor transistors—From planar to nanowire structures", *Mrs Bulletin* **39**, 668, (2014).

[8] K. A. Dick, K. Deppert, M. W. Larsson, T. Mårtensson, W. Seifert, L. R. Wallenberg and L. Samuelson, "Synthesis of branched 'nanotrees' by controlled seeding of multiple branching events", *Nature Materials* **3**, 380 (2004).

[9] M. Heurlin, M. H. Magnusson, D. Lindgren, M. Ek, L. R. Wallenberg, K. Deppert and L. Samuelson, "Continuous gas-phase synthesis of nanowires with tunable properties", *Nature* **492**, 90 (2012).

[10] Z. Bi, A. Gustafsson, F. Lenrick, D. Lindgren, O. Hultin, L. R. Wallenberg, B. J. Ohlsson, B. Monemar and L. Samuelson, "High In-content InGaN nano-pyramids: Tuning crystal homogeneity by optimized nucleation of GaN seeds", *Journal of Applied Physics* **123**, 025102 (2018).

[11] R. G. Hobbs, N. Petkov and J. D. Holmes, "Semiconductor Nanowire Fabrication by Bottom-up and Top-Down Paradigms", *Chemistry of Materials* **24**, 1975 (2012).

[12] T. Mårtensson, P. Carlberg, M. Borgström, L. Montelius, W. Seifert and L. Samuelson, ”Nanowire arrays defined by nanoimprint lithography”, *Nano letters* **4**, 699 (2004).

[13] K. Dick, “Epitaxial Growth and Design of Nanowires and Complex Nanostructures”, Doctoral Thesis, Division of Solid State Physics, Lund University, Lund, Sweden (2007).

[14] M. Heurlin, M. H. Magnusson, D. Lindgren, M. Ek, L. R. Wallenberg, K. Deppert and L. Samuelson, “Continuous gas-phase synthesis of nanowires with tunable properties”, *Nature* **492**, 90 (2012).

[15] R. W. Johnson, A. Hultqvist and S. F. Bent, “A brief review of atomic layer deposition: from fundamentals to applications”, *Materials today* **17**, 236 (2014).

[16] A. K. Shalek, J. T. Robinson, E. S. Karp, J. S. Lee, D.-R. Ahn, M.-H. Yoon, A. Sutton, M. Jorgolli, R. S. Gertner, T. S. Gujral, G. MacBeath, E. G. Yang and H. Park, “Vertical silicon nanowires as a universal platform for delivering biomolecules into living cells”, *Proceedings of the National Academy of Sciences* **107**, 1870 (2010).

[17] C. Eriksson Linsmeier, C. N. Prinz, L. M. E. Pettersson, P. Caroff, L. Samuelson, J. Schouenborg, L. Montelius, N. Danielsen, “Nanowire Biocompatibility in the Brain-Looking for a Needle in a 3D Stack”, *Nano letters* **9**, 4184 (2009).

[18] D. Holbrook, W. M. Cohen, D. A. Hounshell and S. Klepper, “The nature, sources, and consequences of firm differences in the early history of the semiconductor industry”, *Strategic Management Journal* **21**, 10 (2000).

[19] S. M. Sze and M.-K. Lee, “Semiconductor devices: physics and technology”, John Wiley & Sons inc. (2008).

[20] J. A. del Alamo, “Nanometre-scale electronics with III–V compound semiconductors”, *Nature* **479**, 317 (2011).

[21] K. L. Kavanagh, “Misfit dislocations in nanowire heterostructures”, *Semiconductor Science and Technology* **25**, 024006 (2010).

[22] C. Ronning, C. Borschel, S. Geburt, and R. Niepelt, “Ion beam doping of semiconductor nanowires”, *Materials Science and Engineering: R: Reports* **70**, 30 (2010).

[23] J. Wallentin, and M. T. Borgström, ”Doping of semiconductor nanowires”, *Journal of Materials Research* **26**, 2142 (2011).

[24] W. Mönch, “Occupation of Surface States and Surface Band-Bending in Thermal Equilibrium” In: “Semiconductor Surfaces and Interfaces”, *Springer Series in Surface Sciences*, **26**. Springer, Berlin, Heidelberg, (1995).

[25] L. Lin and J. Robertson, “Defect states at III-V semiconductor oxide interfaces”, *Applied Physics Letters* **98**, 082903 (2011).

[26] B. Brennan, and G. Hughes, "Identification and thermal stability of the native oxides on InGaAs using synchrotron radiation based photoemission", *Journal of Applied Physics* **108**, 053516 (2010).

[27] R. Timm, M. Hjort, A. Fian, B. M. Borg, C. Thelander, J. N. Andersen, L.-E. Wernersson, and A. Mikkelsen, ”Interface composition of InAs nanowires with $Al_2O_3$ and $HfO_2$ thin films”, *Applied Physics Letters* **99**, 222907 (2011).

[28] M. Houssa, E. Chagarov and A. Kummel, “Surface defects and passivation of Ge and III–V interfaces”, *Mrs Bulletin* **34**, 504 (2009).

[29] G. Otnes and M. T. Borgström, ”Towards high efficiency nanowire solar cells”, *Nano today* **12**, 31 (2017).

[30] M. Hjort, ”III-V Nanowire Surfaces”, Doctoral Thesis, Division of Synchrotron Radiation Research, Lund University, Lund, Sweden, (2014).

[31] J. V. Knutsson, ”Atomic scale characterization of III-V nanowire surfaces”, Doctoral Thesis, Division of Synchrotron Radiation Research, Lund University, Lund, Sweden, 2017.

[32] R. Anton, T. Wiegner, W. Naumann, M. Liebmann and C. Klein, “Design and performance of a versatile, cost-effective microwave electron cyclotron resonance plasma source for surface and thin film processing”, *Review of Scientific Instruments* **71**, 1177 (2000).

[33] Z. Lu, Y. Jiang, W. I. Wang, M. C. Teich and R. M. Osgood Jr., “GaSb-oxide removal and surface passivation using an electron cyclotron resonance hydrogen source”, *Journal of Vacuum Science & Technology B* **10**, 1856 (1992).

[34] A. D. Carter, W. J. Mitchell, B. J. Thibeault, J. J. M. Law and M. J. W. Rodwell “$Al_2O_3$ Growth on (100) $In_{0.53}Ga_{0.47}As$ Initiated by Cyclic Trimethylaluminum and Hydrogen Plasma Exposures”, *Applied Physics Express* **4**, 091102 (2011).

[35] J. Johansson and K. A. Dick, “Recent advances in semiconductor nanowire heterostructures”, *CrystEngComm* **13**, 7175 (2011).

[36] A. Zhang, G. Zheng and C. M. Lieber, “Nanowires: Building Blocks for Nanoscience and Nanotechnology”, Springer International Publishing Switzerland (2016).

[37] R. Treuting and S. Arnold, “Orientation habits of metal whiskers”, *Acta Metallurgica* **5**, 598 (1957).

[38] T. Mårtensson, C. P. T. Svensson, B. A. Wacaser, M. W. Larsson, W. Seifert, K. Deppert, A. Gustafsson, L. R. Wallenberg and L. Samuelson, ”Epitaxial III-V Nanowires on Silicon”, *Nano Letters* **4**, 1987, (2004).

[39] K. Tomioka, M. Yoshimura and T. Fukui, “A III–V nanowire channel on silicon for high-performance vertical transistors”, *Nature* **488**, 189 (2012).

[40] B. Mandl, J. Stangl, E. Hilner, A. A. Zakharov, K. Hillerich, A. W. Dey, L. Samuelson, G. Bauer, K. Deppert and A. Mikkelsen, “Growth mechanism of self-catalyzed group III− V nanowires”, *Nano letters* **10**, 4443 (2010).

[41] C. Lindberg, A. Whiticar, K. A. Dick, N. Sköld, J. Nygård and J. Bolinsson, “Silver as Seed-Particle Material for GaAs Nanowires - Dictating Crystal Phase and Growth Direction by Substrate Orientation”, *Nano letters* **16**, 2181 (2016).

[42] K. A. Dick and P. Caroff, “Metal-seeded growth of III–V semiconductor nanowires: towards gold-free synthesis”, *Nanoscale* **6**, 3006 (2014).

[43] A. Troian, “Synchrotron X-ray based characterization of technologically relevant III-V surfaces and nanostructures”, Doctoral Thesis, Division of Synchrotron Radiation Research, Lund University, Lund, Sweden, (2019).

[44] D. Spirkoska, C. Colombo, M. Heiss, G. Abstreiter and A. F. i Morral, “The use of molecular beam epitaxy for the synthesis of high purity III–V nanowires”, *Journal of Physics: Condensed Matter* **20**, 454225 (2008).

[45] P. Gibart, "Metal organic vapour phase epitaxy of GaN and lateral overgrowth", *Reports on Progress in Physics* **67**, 667 (2004).

[46] K. Deppert, J.-O. Bovin, J.-O. Malm and L. Samuelson, “A new method to fabricate size-selected compound semiconductor nanocrystals: aerotaxy”, *Journal of Crystal Growth* **169**, 13 (1996).

[47] K. Deppert, M. H. Magnusson, L. Samuelson, J.-O. Malm, C. Svensson and J.-O. Bovin, “Size-selected nanocrystals of III–V semiconductor materials by the aerotaxy method”, *Journal of Aerosol Science* **29**, 737 (1998).

[48] W. Metaferia, A. R. Persson, K. Mergenthaler, F. Yang, W. Zhang, A. Yartsev, R. Wallenberg, M.-E. Pistol, K. Deppert, L. Samuelson and M. H. Magnusson, “GaAsP Nanowires Grown by Aerotaxy”, *Nano Letters* **16**, 5701 (2016).

[49] S. Yngman, S. R. McKibbin, J. V. Knutsson, A. Troian, F. Yang, M. H. Magnusson, L. Samuelson, R. Timm and A. Mikkelsen, “Surface smoothing and native oxide suppression on Zn doped aerotaxy GaAs nanowires”, *Journal of Applied Physics* **125**, 025303 (2019).

[50] F. Yang, M. E. Messing, K. Mergenthaler, M. Ghasemi, J. Johansson, L. R. Wallenberg, M.-E. Pistol, K. Deppert, L. Samuelson and M. H. Magnusson, “Zn-doping of GaAs nanowires grown by Aerotaxy”, *Journal of Crystal Growth* **414**, 181 (2015).

[51] W. Metaferia, S. Sivakumar, A. R. Persson, I. Geijselaers, L. R. Wallenberg, K. Deppert, L. Samuelson and M. H. Magnusson, “*n*-type doping and morphology of GaAs nanowires in Aerotaxy”, *Nanotechnology* **29**, 285601 (2018).

[52] E. Barrigón, O. Hultin, D. Lindgren, F. Yadegari, M. H. Magnusson, L. Samuelson, L. I. M. Johansson and M. T. Björk, ”GaAs Nanowire *pn*-Junctions Produced by Low-Cost and High-Throughput Aerotaxy”, *Nano Letters* **18**, 1088 (2018).

[53] W. Zhang, F. Yang, M. E. Messing, K. Mergenthaler, M.-E. Pistol, K. Deppert, L. Samuelson, M. H. Magnusson and A. Yartsev,” Recombination dynamics in aerotaxy-grown Zn-doped GaAs nanowires”, *Nanotechnology* **27**, 455704 (2016).

[54] D. Tabor, “Mohs's hardness scale-a physical interpretation”, *Proceedings of the Physical Society. Section B* **67**, 249 (1954).

[55] G. V. Samsonov, “Handbook of the Physicochemical Properties of the Elements”, Springer, USA (1986).

[56] P. W. Hawkes and J. C. H Spence, “Science of Microscopy”, Springer Science and Business Media, USA (2007).

[57] J. Tersoff and D. R. Hamann, “Theory and application for the scanning tunneling microscope”, *Physical review letters* **50**, 1998 (1983).

[58] H. J. Reittu, “Fermi’s golden rule and Bardeen’s tunneling theory”, *American Journal of Physics* **63**, 940 (1995).

[59] J. Tersoff and D. R. Hamann, "Theory of the Scanning Tunneling Microscope", *Physical Review B* **31**, 805 (1985).

[60] R. M. Feenstra, J. A. Stroscio, J. Tersoff and A. P. Fein, “Atom-selective imaging of the GaAs (110) surface”, *Physical review letters* **58**, 1192 (1987).

[61] J. P. Ibe, P. P. Bey Jr., S. L. Brandow, R. A. Brizzolara, N. A. Burnham, D. P. DiLella, K. P. Lee, C. R. K. Marrian and R. J. Colton, “On the electrochemical etching of tips for scanning tunneling microscopy”, *Journal of Vacuum Science & Technology A* **8**, 3570 (1990).

[62] E. Lassner, W.-D. Schubert, “Tungsten: Properties, Chemistry, Technology of the Element, Alloys, and Chemical Compounds”, p.54, Springer, USA (1999).

[63] G. Binnig, C. F. Quate and C. Gerber, “Atomic force microscope”, *Physical review letters* **56**, 930 (1986).

[64] H. Ueyama, M. Ohta, Y. Sugawara and S. Morita, ”Atomically resolved InP (110) surface observed with noncontact ultrahigh vacuum atomic force microscope”, *Japanese journal of applied physics* **34**, L1086 (1995).

[65] G. Haugstad, “Atomic Force Microscopy: Understanding Basic Modes and Advanced Applications”, John Wiley and Sons inc., USA (2012).

[66] N. Jalili and K. Laxminarayana, “A review of atomic force microscopy imaging systems: application to molecular metrology and biological sciences”, *Mechatronics* **14**, 907 (2004).

[67] R. A. Oliver, ”Advances in AFM for the electrical characterization of semiconductors”, *Reports on Progress in Physics* **71**, 076501 (2008).

[68] S. N. Magonov, V. Elings and M.-H. Whangbo, “Phase imaging and stiffness in tapping-mode atomic force microscopy”, *Surface Science* **375**, L385 (1997).

[69] H. Hertz, ”Ueber einen Einfluss des ultravioletten Lichtes auf die electrische Entladung”, *Annalen Der Physik* **31**, 983, (1887).

[70] A. Einstein, “Generation and conversion of light with regard to a heuristic point of view”, *Annalen Der Physik* **17**, 132 (1905).

[71] S. Hüfner, “Photoelectron Spectroscopy: principles and applications”, Springer: Berlin (2003).

[72] P. Shayesteh, “Atomic Layer Deposition and Immobilised Molecular Catalysts Studied by In and Ex Situ Electron Spectroscopy”, Doctoral Thesis, Division of Synchrotron Radiation Research, Lund University, Lund, Sweden, 2019.

[73] N. Johansson, “Synchrotron-based *In-Situ* Electron Spectroscopy Applied to Oxide Formation and Catalysis”, Doctoral Thesis, Division of Synchrotron Radiation Research, Lund University, Lund, Sweden, 2018.

[74] J. W. Niemantsverdriet, “Spectroscopy in Catalysis: an introduction”, WILEY-VCH Verlag, Weinheim, third edition, (2007).

[75] R. Nyholm, J. N. Andersen, U. Johansson, B.N. Jensen and I. Lindau, “Beamline I311 at MAX-LAB: a VUV/soft X-ray undulator beamline for high resolution

electron spectroscopy", *Nuclear Instruments and Methods in Physics Research A* **467–468**, 520 (2001).

[76] N. Mårtensson, P. Baltzer, P.A. Briihwiler, J.-O. Forsell, A. Nilsson, A. Stenborg and B. Wannberg, "A very high resolution electron spectrometer", *Journal of Electron Spectroscopy and Related Phenomena* **70**, 117 (1994).

[77] P. Van Vaerenbergha, J. Léonardon, M. Sztucki, P. Boesecke, J. Gorini, L. Claustre, F. Sever, J. Morse and T. Narayanan, "An upgrade beamline for combined wide, small and ultra small-angle x-ray scattering at the ESRF", *AIP Conference Proceedings* **1741**, 030034 (2016).

[78] A.G. Kikhney and D.I. Svergun, "A practical guide to small angle X-ray scattering (SAXS) of flexible and intrinsically disordered proteins", *FEBS Letters* **589**, 2570 (2015).

[79] H. Ko, K. Takei, R. Kapadia, S. Chuang, H. Fang, P. W. Leu, K. Ganapathi, E. Plis, H. S. Kim, S. Y. Chen, M. Madsen, A. C. Ford, Y. L. Chueh, S. Krishna, S. Salahuddin and A. Javey, "Ultrathin compound semiconductor on insulator layers for high-performance nanoscale transistors", *Nature* **468**, 286 (2010).

[80] J. Wu, A. S. Babadi, D. Jacobsson, J. Colvin, S. Yngman, R. Timm, E. Lind and L.-E. Wernersson, "Low Trap Density in InAs/High-k Nanowire Gate Stacks with Optimized Growth and Doping Conditions", *Nano Letters* **16**, 2418 (2016).

[81] J. Svensson, A. W. Dey, D. Jacobsson and L.-E. Wernersson, "III-V Nanowire Complementary Metal-Oxide Semiconductor Transistors Monolithically Integrated on Si", *Nano Letters* **15**, 7898 (2015).

[82] E. Memišević, J. Svensson, M. Hellenbrand, E. Lind and L.-E. Wernersson, "Scaling of Vertical InAs-GaSb Nanowire Tunneling Field-Effect Transistors on Si", IEEE *Electron Device Letters* **37**, 549 (2016).

[83] L. B. Ruppalta, E. R. Cleveland, J. G. Champlain, S. M. Prokes, J. B. Boos, D. Park and B. R. Bennett, "Atomic layer deposition of $Al_2O_3$ on GaSb using in situ hydrogen plasma exposure", *Applied Physics Letters* **101**, 231601 (2012).

[84] M. Barth, G. B. Rayner Jr., S. McDonnell, R. M. Wallace, B. R. Bennett, R. Engel-Herbert and S. Datta, "High quality $HfO_2$/p-GaSb(001) metal-oxide-semiconductor capacitors with 0.8 nm equivalent oxide thickness", *Applied Physics Letters* **105**, 222103 (2014).

[85] D. M. Zhernokletov, H. Dong, B. Brennan, M. Yakimov, V. Tokranov, S. Oktyabrsky, J. Kim and R. M. Wallace, "Surface and interfacial reaction study of half cycle atomic layer deposited $HfO_2$ on chemically treated GaSb surfaces", *Applied Physics Letters* **102**, 131602 (2013).

[86] S. McDonnell, B. Brennan, E. Bursa, R. M. Wallace, K. Winkler and P. Baumann, "GaSb oxide thermal stability studied by dynamic-XPS", *Journal of Vacuum Science and Technology B* **32**, 041201 (2014).

[87] L. Samuelson, J. Lindahl, L. Montelius and M.-E. Pistol, "Tunnel-Induced Photon Emission in Semiconductors Using an STM", *Physica Scripta* **T42**, 149 (1992).

[88] K. Flöhr, K. Sladek, H. Y. Günel, M. I. Lepsa, H. Hardtdegen, M. Liebmann, T. Schäpers and M. Morgenstern, "Scanning tunneling microscopy with InAs nanowire tips", *Applied Physics Letters* **101**, 243101 (2012).

[89] H. S. Wong, S. C. Tan, N. Wang and C. Durkan, "Hydrothermally-Grown ZnO Nanowire Tips for Scanning Tunneling Microscopy", *Journal of Nanoscience and Nanotechnology* **12,** 2394 (2012).

[90] M. Pelliccione, A. Jenkins, P. Ovartchaiyapong, C. Reetz, E. Emmanouilidou, N. Ni and A. C. Bleszynski Jayich, "Scanned probe imaging of nanoscale magnetism at cryogenic temperatures with a single-spin quantum sensor", *Nature Nanotechnology* **11**, 700 (2016).

[91] M. Behzadirad, M. Nami, A. K. Rishinaramagalam, D. F. Feezell and T. Busani, "GaN nanowire tips for nano scale atomic force microscopy", *Nanotechnology* **28**, 20LT01 (2017).

[92] J. C. Weber, P. T. Blanchard, A. W. Sanders, J. C. Gertsch, S. M. George, S. Berweger, A. Imtiaz, K. J. Coakley, T. M. Wallis, K. A. Bertness, P. Kabos, N. A. Sanford and V. M. Bright, "GaN nanowire coated with atomic layer deposition of tungsten: a probe for near-field scanning microwave spectroscopy", *Nanotechnology* **25**, 415502 (2014).

[93] K. Prabhakaran, T. G. Andersson and K. Nozawa, "Nature of native oxide on GaN surface and its reaction with Al", *Applied Physics Letters* **69**, 3212 (1996).

[94] N. J. Watkins, G. W. Wicks and Y. Gao, "Oxidation study of GaN using X-ray photoemission spectroscopy", *Applied Physics Letters* **75**, 2602 (1999).

[95] T. Yamada, J. Ito, R. Asahara, K. Watanabe, M. Nozaki, S. Nakazawa, Y. Anda, M. Ishida, T. Ueda, A. Yoshigoe, T. Hosoi, T. Shimura and H. Watanabe, "Comprehensive study on initial thermal oxidation of GaN(0001) surface and subsequent oxide growth in dry oxygen ambient", *Journal of applied physics* **121**, 035303 (2017).

[96] G. Zeng, C.-K. Tan, N. Tansu, and B. A. Krick, "Ultralow wear of gallium nitride", *Applied Physics Letters* **109**, 051602 (2016).

[97] S. D. Hersee, X. Sun and X. Wang, "The Controlled Growth of GaN Nanowires", *Nano Letters* **68**, 1808, (2006).

[98] F. Qian, S. Gradecak, Y. Li, C. Y. Wen and C. M. Lieber, "Core/multishell nanowire heterostructures as multicolor, high-efficiency light-emitting diodes", *Nano letters* **5**, 2287 (2005).